AGU PUBLICATIONS

JGR

Journal of Geophysical Research: Atmospheres

RESEARCH ARTICLE

10.1002/2017JD026781

Key Points:
- In situ measurements of the CH_2O/NO_2 ratio are a good indicator of ozone sensitivity but are spatially limited in their coverage
- Column measurements of CH_2O/NO_2 are a poor indicator of near-surface ozone sensitivity due to uneven vertical mixing in the lower troposphere
- Long- and short-term observations of changes in column CH_2O/NO_2 ratios may still provide useful information about the relative importance of O_3 precursors

Supporting Information:
- Supporting Information S1
- Figure S1

Correspondence to:
J. R. Schroeder,
jason.r.schroeder@nasa.gov

Citation:
Schroeder, J. R., et al. (2017), New insights into the column CH_2O/NO_2 ratio as an indicator of near-surface ozone sensitivity, *J. Geophys. Res. Atmos.*, *122*, 8885–8907, doi:10.1002/2017JD026781.

Received 10 MAR 2017
Accepted 11 JUL 2017
Accepted article online 15 JUL 2017
Published online 17 AUG 2017

New insights into the column CH_2O/NO_2 ratio as an indicator of near-surface ozone sensitivity

Jason R. Schroeder[1,2], James H. Crawford[1], Alan Fried[3], James Walega[3], Andrew Weinheimer[4], Armin Wisthaler[5,6], Markus Müller[5], Tomas Mikoviny[6], Gao Chen[1], Michael Shook[1], Donald R. Blake[7], and Gail S. Tonnesen[8]

[1]NASA Langley Research Center, Hampton, Virginia, USA, [2]NASA Postdoctoral Program, NASA Langley Research Center, Hampton, Virginia, USA, [3]Institute of Arctic and Alpine Research, University of Colorado Boulder, Boulder, Colorado, USA, [4]National Center for Atmospheric Research, Boulder, Colorado, USA, [5]Institute of Ion Physics and Applied Physics, University of Innsbruck, Innsbruck, Austria, [6]Department of Chemistry, University of Oslo, Oslo, Norway, [7]Department of Chemistry, University of California, Irvine, California, USA, [8]US Environmental Protection Agency, Denver, Colorado, USA

Abstract Satellite-based measurements of the column CH_2O/NO_2 ratio have previously been used to estimate near-surface ozone (O_3) sensitivity (i.e., NO_x or VOC limited), and the forthcoming launch of air quality-focused geostationary satellites provides a catalyst for reevaluating the ability of satellite-measured CH_2O/NO_2 to be used in this manner. In this study, we use a 0-D photochemical box model to evaluate O_3 sensitivity and find that the relative rate of radical termination from radical-radical interactions to radical-NO_x interactions (referred to as LRO_x/LNO_x) provides a good indicator of maximum O_3 production along NO_x ridgelines. Using airborne measurements from NASA's Deriving Information on Surface Conditions from Column and Vertically Resolved Observations Relative to Air Quality (DISCOVER-AQ) deployments in Colorado, Maryland, and Houston, we show that in situ measurements of CH_2O/NO_2 can be used to indicate O_3 sensitivity, but there is an important "transition/ambiguous" range whereby CH_2O/NO_2 fails to categorize O_3 sensitivity, and the range and span of this transition/ambiguous range varies regionally. Then, we apply these findings to aircraft-derived column density measurements from DISCOVER-AQ and find that inhomogeneities in vertical mixing in the lower troposphere further degrades the ability of column CH_2O/NO_2 to indicate near-surface O_3 sensitivity (i.e., the transition/ambiguous range is much larger than indicated by in situ data alone), and we hypothesize that the global transition/ambiguous range is sufficiently large to make the column CH_2O/NO_2 ratio unuseful for classifying near-surface O_3 sensitivity. Lastly, we present a case study from DISCOVER-AQ-Houston that suggests that O_3 sensitivity on exceedance days may be substantially different than on nonexceedance days (which may be observable from space) and explore the diurnal evolution of O_3 sensitivity, O_3 production, and the column CH_2O/NO_2 ratio. The results of these studies suggest that although satellite measurements of CH_2O/NO_2 alone may not be sufficient for accurately classifying near-surface O_3 sensitivity, new techniques offered by geostationary platforms may nonetheless provide methods for using space-based measurements to develop O_3 mitigation strategies.

1. Introduction

Exposure to high levels of tropospheric O_3 is deleterious to human health, and at present more than 120 million residents of the U.S. live in regions that are deemed "nonattainment areas" according to the U.S. Environmental Protection Agency's (EPA) national ambient air quality standards (NAAQS) [*U.S. Environmental Protection Agency* (*US EPA*), 2015]. In addition, the EPA has recently lowered the NAAQS exceedance level for O_3 from 75 parts per billion by volume (ppbv) to 70 ppbv, where compliance with the NAAQS is evaluated as the 3 year average of the fourth highest daily 8 h O_3 average in each year. As a result, some regions that were previously in compliance with the O_3 NAAQS may now be considered nonattainment areas, and some previous nonattainment areas are expected to be reclassified with a worse classification, meaning that a larger number of air quality management districts will be required to take action to reduce regional O_3 [*US EPA*, 2016].

Photochemical formation of O_3 occurs through a series of complex, nonlinear reactions involving sunlight, NO_x ($NO_x \equiv NO + NO_2$), volatile organic compounds (VOCs), and free radical species that oxidize both NO_x and VOCs [*Chameides and Walker*, 1973]. Often, local concentrations of either radicals or NO_x are sufficiently high such that the other species is chemically limiting with respect to O_3 formation. These two photochemical

regimes are commonly referred to as NO_x limited and VOC limited [*Kleinman*, 1994; *Sillman et al*., 1990]. A more accurate term for VOC limited is "radical limited" since it is the availability of peroxy radicals resulting from the oxidation of VOCs that controls the rate of O_3 production, rather than the precursor VOCs themselves. Because the NAAQS is based on the maximum daily 8 h average (MDA8) O_3, it is also important to consider the daytime evolution of photochemical regimes. Many urban areas transition from radical-limited conditions in the morning to NO_x-limited conditions in the afternoon [*Tonnesen and Dennis*, 2000], and thus the sensitivity of the MDA8 O_3 to changes in VOC and NO_x precursor emissions is determined by the cumulative production of O_3 and NO_2 during both radical- and NO_x-limited conditions over the course of the day. Understanding the complex spatial and temporal evolution of photochemical regimes at local scales is a crucial piece of information for air quality planners looking to enact effective policies to mitigate O_3 pollution. In this work, we use data collected during NASA's Deriving Information on Surface Conditions from Column and Vertically Resolved Observations Relative to Air Quality (DISCOVER-AQ) field campaign to better understand the strengths and limitations of using column-based measurements of formaldehyde (CH_2O) and nitrogen dioxide (NO_2) to diagnose local photochemical conditions and explore the potential role of future geostationary satellites in monitoring local photochemical regimes at high spatial and temporal resolution.

Many papers have investigated the differences in chemical signatures under NO_x-limited and radical-limited regimes [*Chameides et al*., 1992; *Kleinman*, 1994; *Kleinman et al*., 1995, 1997; *Sillman et al*., 1990, 1995], and a brief summary of their findings is presented here. Peroxy radical (HO_2 + RO_2) formation via the reaction of VOCs with the hydroxyl radical (OH) is the first and often rate-limiting step in O_3 production. O_3 is then produced by subsequent reactions between HO_2 or RO_2 and NO that lead to radical propagation (via subsequent reformation of OH). Radical termination proceeds via reaction of OH with NO_x to form nitric acid (HNO_3, reaction (1), hereafter referred to as LNO_x) or by radical-radical reactions, primarily peroxy-peroxy combination reactions resulting in stable peroxide formation (reactions (2)–(4), hereafter referred to as LRO_x, where $RO_x \equiv RO_2 + HO_2$):

$$OH + NO_2 \rightarrow HNO_3 \quad (1)$$

$$2HO_2 \rightarrow H_2O_2 + O_2 \quad (2)$$

$$HO_2 + RO_2 \rightarrow ROOH + O_2 \quad (3)$$

$$2RO_2 \rightarrow ROOR + O_2 \quad (4)$$

It should be noted that in certain environments, other processes such as alkyl nitrate formation and peroxyacetyl nitrate (PAN) formation can contribute a nonnegligible amount to radical loss [*Kleinman*, 2005]. In high-radical, low-NO_x environments, reactions (2)–(4) remove radicals at a faster rate than reaction (1) (i.e., $LRO_x \gg LNO_x$), and the photochemical regime is said to be "NO_x limited." In low-radical, high-NO_x environments the opposite is true and the regime is said to be "VOC limited," or sometimes referred to as "NO_x saturated" (i.e., $LRO_x \ll LNO_x$). However, it should be noted that O_3 production is only indirectly related to VOCs but instead is directly related to the available radical pool to which VOC oxidation contributes. This distinction is important because the relationship between VOCs and radicals is dependent on external factors such as available solar radiation. For example, one can imagine a low-light environment, such as morning/evening or wintertime, where, although there may be very high VOC loadings, O_3 production is limited by the availability of peroxy radicals to convert NO to NO_2. In this situation, the term VOC limited is inadequate, as O_3 production is technically radical limited. Therefore, in this work, the commonly used term VOC limited will be replaced by the more accurate term radical limited and is taken to have the same meaning as NO_x saturated. Perhaps a more accurate term is "RO_x limited" since NO_2 itself is a radical, and thus reaction (1) is technically a "radical-radical" interaction. In this work, "radicals" is taken to refer to the RO_x family of radicals, which follows terminology used in recent literature [*Duncan et al*., 2010; *Edwards et al*., 2013]. When the rates of the two loss processes are equal (that is, $Rate_1 = Rate_2 + Rate_3 + Rate_4$, or $LNO_x = LRO_x$), the regime is said to be at the photochemical transition point, and O_3 production is expected to be equally sensitive to changes in both VOCs and NO_x [*Kleinman*, 1994; *Kleinman et al*., 1997; *Sillman et al*., 1990]. In this work, the relationship between these two competing radical termination processes will be evaluated as the ratio LRO_x/LNO_x.

A complete evaluation of local photochemical regimes using the LRO_x/LNO_x ratio typically requires simultaneous, high-frequency measurements of myriad trace gases and radical species and is beyond the scope of typical air quality monitoring stations. Because of this, much work has focused on using measurements of commonly measured trace gases as indicators of photochemical regime [*Sillman*, 1995; *Sillman and Samson*, 1995; *Sillman et al*., 1998; *Tonnesen and Dennis*, 2000; *Xie et al*., 2014]. CH_2O is a short-lived ($\tau \approx 1$–3 h at midday) oxidation product of most VOCs, and during the daytime its mixing ratio is often correlated with the OH rate constant weighted VOC reactivity (VOCR) and the rate of peroxy radical formation [*Parrish et al*., 2012; *Sillman*, 1995; *Valin et al*., 2015; *Wolfe et al*., 2015]. *Tonnesen and Dennis* [2000] found that in situ measurements of the CH_2O/NO_2 ratio could be used to diagnose local photochemical regimes, with ratios <0.8 indicating a radical-limited environment, ratios >1.8 indicating a NO_x-limited environment, and ratios between 0.8 and 1.8 indicating a "transition" environment where O_3 was equally sensitive to radicals and NO_x. While in situ measurements of indicator species (such as CH_2O/NO_2) provide a more easily accessible method of monitoring O_3 sensitivity, sparse networks of surface monitoring sites cannot realistically capture the spatial heterogeneity of O_3 sensitivity in urban areas. Satellite measurements, on the other hand, provide measurements over large spatial areas, although the viability of satellite measurements in diagnosing O_3 sensitivity is deserving of further scrutiny.

Over polluted areas, both CH_2O and NO_2 have vertical distributions that are heavily weighted toward the lower troposphere, meaning that satellite measurements of these gases are fairly representative of near-surface conditions. Many studies have taken advantage of these favorable vertical distributions to investigate surface emissions of NO_x and VOCs from space [*Boersma et al*., 2009; *Martin et al*., 2004; *Millet et al*., 2008; *Streets et al*., 2013]. *Martin* [2004] was the first to use satellite measurements of the ratio of CH_2O/NO_2 to explore near-surface O_3 sensitivities from space. Using a global chemical transport model, *Martin* [2004] estimated that the transition between radical- and NO_x-limited regimes occurred at a CH_2O/NO_2 ratio of 1, with ratios >1 being NO_x limited and ratios <1 being radical limited. *Duncan et al*. [2010] used a combination of regional chemical transport modeling and box modeling in southern California to show a similar result to *Tonnesen and Dennis* [2000]: the CH_2O/NO_2 ratio can be used to indicate O_3 sensitivity, but there is a range of CH_2O/NO_2 values that fall within a "transition/ambiguous" region. *Duncan et al*. [2010] found this transition/ambiguous range to be $1 < CH_2O/NO_2 < 2$). *Duncan et al*. [2010] then applied their findings to satellite measurements from the Ozone Monitoring Instrument (OMI, housed aboard NASA's Aura satellite) and found that with the exception of a handful of large cities, most of the U.S. had column CH_2O/NO_2 ratios >2 and were classified as NO_x limited. However, *Duncan et al*. [2010] focused on the period 2005–2007 and do not account for reductions in NO_x emissions under the EPA's 2008 NAAQS State Implementation Plan (SIP) requirements [*US EPA*, 2008]. Recent papers have applied the findings of *Duncan et al*. [2010] to observe O_3 sensitivity in other parts of the world [*Choi et al*., 2012; *Jin and Holloway*, 2015; *Mahajan et al*., 2015; *Witte et al*., 2011].

While any information about near-surface O_3 sensitivity is relevant for air quality policymakers, the polar orbit of OMI only allows for measurement once per day—usually around solar noon—and exploration of diurnal variability in the column CH_2O/NO_2 ratio would be invaluable in drafting more effective O_3 reduction policies. Additionally, the large footprint sizes of current polar-orbiting satellites often are not adequate to resolve spatial gradients between urban and suburban areas unless long-term averaging is used to reduce effective pixel size. This long-term averaging may conceal useful information about differences in O_3 sensitivities on exceedance days versus nonexceedance days and inhibits the ability of policymakers to observe changes in O_3 sensitivity during short-term and multiday O_3 exceedance events. A new collection of geostationary air quality satellites is on the horizon that will address the problem of temporal resolution while simultaneously delivering improved spatial resolution. These include the Tropospheric Emissions: Monitoring of Pollution (TEMPO) mission over North America (http://science.nasa.gov/missions/tempo/), Sentinel-4 over Europe and North Africa (http://www.esa.int/Our_Activities/Observing_the_Earth/Copernicus/Sentinels_-4_-5_and_-5P), and the Geostationary Environment Monitoring Spectrometer (GEMS) over East Asia (http://www.ball.com/aerospace/programs/gems). The geostationary orbit of TEMPO, for example, will allow for observation of the CH_2O/NO_2 ratio with a 3 h resolution. In anticipation of these geostationary air quality observations, NASA sponsored a series of field studies under the DISCOVER-AQ project to examine the relationship between surface air quality and the vertical distribution of pollutants as they would be observed from space. Having conducted more than 800 soundings of lower atmospheric composition over areas of nonattainment, the

DISCOVER-AQ data set enables the exploration of relationships between column amounts of O_3, NO_2, and CH_2O with very high spatial and temporal resolution, which effectively affords us a preview of the potential utility and applicability of future geostationary satellite missions. In the work presented here, airborne trace gas measurements and box modeling are used to evaluate (1) the relationship between LRO_x/LNO_x and O_3 production sensitivity, (2) the relationship between CH_2O/NO_2 and LRO_x/LNO_x, and (3) the ability of column CH_2O/NO_2 ratios to indicate near-surface O_3 sensitivity.

2. Methods

2.1. Overview of DISCOVER-AQ

DISCOVER-AQ was a four-part field campaign with deployments in Maryland (June–July 2011), California's San Joaquin Valley (January–February 2013), Houston, Texas (September 2013), and the northern Front Range area of Colorado (July–August 2014). Currently, each of these four locations consistently violates the NAAQS for O_3 (with respect to O_3, Houston and Colorado are listed as "marginal," northern Maryland is listed as "moderate," and much of California's San Joaquin Valley is listed as "extreme" at the time of this publication). Although California's San Joaquin Valley is plagued by O_3 exceedances during summer, the wintertime deployment was intended to study particulate matter, so data from the California deployment of DISCOVER-AQ are not immediately relevant for this study. During each deployment, the NASA P-3B aircraft was used to consistently and repeatedly fly soundings (spirals) over specific sites. These sites were situated in the heart of urban areas, in nearby suburban areas, and outlying rural areas. Weather permitting, spirals were flown over each site with altitudes ranging from ~300 to 4000 m above ground level. At select locations with small airports nearby, missed approaches enabled sampling down to altitudes as low as 30 m. On a typical research flight the P-3B would fly three sorties, spiraling over each site three times (typically in the morning, around midday, and in the afternoon), allowing for observations of vertical distributions over a diurnal scale. Colorado had the highest number of research flights flown (16) and Houston the least (9) with California (10) and Maryland (14) falling in between. Because the primary objective of DISCOVER-AQ was to provide vertical measurements in support of future satellite missions, flights were typically conducted under clear-sky or partly cloudy conditions. Airborne measurements of species that are related to satellite-based platforms and are directly related to this work include O_3, NO_2, and CH_2O. Measurements of other species (water vapor, carbon monoxide (CO), methane (CH_4), carbon dioxide (CO_2), nitric oxide (NO), and VOCs) were used to further aid in analysis. Additional information, including maps of each DISCOVER-AQ study region and descriptions of relevant instrumentation is provided in *Schroeder et al*. [2016].

Column densities of CH_2O and NO_2 were calculated by integrating P-3B 1 s measurements made over the altitude range of each spiral. An in-depth description of the process used to calculate column densities is provided in *Schroeder et al*. [2016], and a brief overview of some of the assumptions used is presented here. Because the maximum altitude reached during each spiral varied, all spirals were normalized to a maximum altitude for each deployment. Spirals that terminated below this normalized altitude were extrapolated upward, and spirals that extended beyond this range were truncated. Upward extrapolation was necessary for 22% of the spirals with the average amount of upward extrapolation being only 30 m, about 1% of the total spiral range. All spirals were also extrapolated down to the surface using measurements from the bottom of each spiral (typically ~300 m above ground level) and assuming a constant mixing ratio down to the surface (i.e., the "column_air" approach described in *Flynn et al*. [2014]). Based on data from spirals with missed approaches, it was estimated that extrapolating down to the surface introduces an uncertainty of ±3% to each calculated column density. The uncertainty for in situ measurements of CH_2O was typically ±100 pptv (parts per trillion by volume) and was ± (20 pptv + 10%) for NO_2. These uncertainties translate to column uncertainties of about ±0.02 Dobson units (DU) for both species and an uncertainty of about 20% for column CH_2O/NO_2 ratios in Colorado and about 15% in Maryland and Houston where ambient CH_2O mixing ratios were higher than in Colorado.

2.2. The Langley Research Center Photochemical Box Model

The observationally constrained NASA Langley Research Center (LaRC) time-dependent photochemical box model was used to simulate chemistry during DISCOVER-AQ. The model is constrained by inputs of trace gases such as O_3, NO, CO, CH_4, CH_2O, water vapor, and other nonmethane hydrocarbons by meteorological parameters such as temperature and pressure and by measured photolysis rates. The model calculates the

diurnal steady state profiles of radicals and other computed species for each set of measurements [*Crawford et al*., 1999; *Olson et al*., 2001, 2006]. In effect, the "model time" runs forward until all radical species are in diurnal equilibrium, and modeled concentrations of each species are explicitly calculated. A complete list of all reactions used in the model is provided in the supporting information. The appropriateness of the equilibrium assumption can be a problem when short-lived species dominate the model photochemistry, e.g., highly reactive VOCs such as biogenic isoprene or alkenes from industrial sources [*Fried et al*., 2011]. The intricacies of the relationship between model assumptions in proximity to such sources as observed during DISCOVER-AQ are expanded upon in *Schroeder et al*. [2016]. Additional model uncertainties arise from uncertainties in measured constraints and uncertainties in kinetic and photolytic rates.

When available, moving 10 s averages of data from P-3B 1 s data merges (available at http://www-air.larc.nasa.gov/missions/discover-aq/discover-aq.html) were used as model inputs. Many nonmethane hydrocarbons (NMHCs) that are model inputs were not measured during DISCOVER-AQ, including propane, C_{4+} alkanes, ethene, ethyne, and ethanol. To estimate these missing inputs, correlations were made between species that were measured during DISCOVER-AQ and missing NMHC inputs that were measured during other field campaigns that were colocated in space and time. University of California Irvine's Whole Air Sampler (WAS) instrument—which routinely measures 75+ NMHCs—flew on board the NASA DC-8 during the SEAC^{4}RS field campaign (Studies of Emissions and Atmospheric Composition, Clouds, and Climate Coupling by Regional Surveys, Houston, August–September 2013) and the FRAPPE field campaign (Front Range Air Pollution and Photochemistry Experiment, Colorado, August 2014) [*Colman et al*., 2001; *Schroeder et al*., 2014; *Simpson et al*., 2010]. An example of this estimation process is provided here: within the FRAPPE data set, it was noted that ethane (which was measured during DISCOVER-AQ-Colorado) and propane (which was not measured during DISCOVER-AQ-Colorado) had a strong linear correlation. This linear relationship was then applied to the Colorado DISCOVER-AQ data set to estimate propane mixing ratios. The portion of the total VOCR that was required to be estimated was typically less than 20%. Further information about this process, including plots of these correlations, is provided in *Schroeder et al*. [2016].

The accuracy of the model in predicting NO_x and radical budgets can be diagnosed by comparing species where model and measurement overlap; i.e., comparing model-calculated species to species that were also measured on the P-3B. In the DISCOVER-AQ data sets, the only overlapping species was NO_2 (CH_2O was used to constrain the model), and model-measurement agreement was evaluated for NO_2 in Colorado, Maryland, and Houston. During FRAPPE, which included measurement of short-lived radical species, model-measurement agreement was evaluated for NO_2 and HO_2. Although the FRAPPE data set is not the primary focus of this work, its colocation in space and time with the DISCOVER-AQ Colorado deployment can provide a good indication of the model's general performance in calculating radical species. In the supporting information accompanying this work, Figures S1 and S2 show model-measurement agreement for NO_2 and HO_2 from FRAPPE. In both cases, slopes near 1 were observed along with good correlations ($r^2 = 0.60$ for HO_2 and $r^2 = 0.96$ for NO_2), indicating that the model was able to reproduce the NO_x and radical environment during FRAPPE. The median NO_2 model-measurement percent difference was 0.3%, with the mode occurring at 0%, and the median HO_2 model-measurement percent difference was −6%, with a mode of −10%. Figure S3 shows plots of modeled and measured NO_2 from DISCOVER-AQ Colorado, Maryland, and Houston. In each deployment, there was generally good agreement between modeled and measured NO_2.

The model was used to calculate additional parameters, such as $P(O_3)$, LRO_x, LNO_x, and VOCR. Here we define $P(O_3)$ as the net rate of production of O_x ($O_x \equiv O_3 + NO_2$), i.e., the difference between the instantaneous rates of formation and destruction. Here the rate of formation is the sum of the rates of all reactions that convert NO to NO_2 without consuming O_3, such as the reaction of HO_2 + NO and RO_2 + NO. The rate of loss of O_3 is the sum of all reactions that remove O_x, such as O_3 photolysis followed by reaction of $O(^1D)$ with water vapor, the direct removal of O_3 by chemical reaction (with OH, HO_2, and alkenes), and the formation of HNO_3 (i.e., reaction (1)). As described above, LNO_x was calculated as the rate of radical loss due to reaction with NO_x, and LRO_x the net rate of radical loss due to radical-radical interactions that create stable peroxides. VOCR was calculated as the sum of the product of the rate constant for the reaction between each model input VOC and OH ($k_{i,OH}$) multiplied by its concentration, $[VOC]_i$:

$$\mathrm{VOCR} = \sum_i k_{i,\mathrm{OH}}[\mathrm{VOC}]_i \tag{5}$$

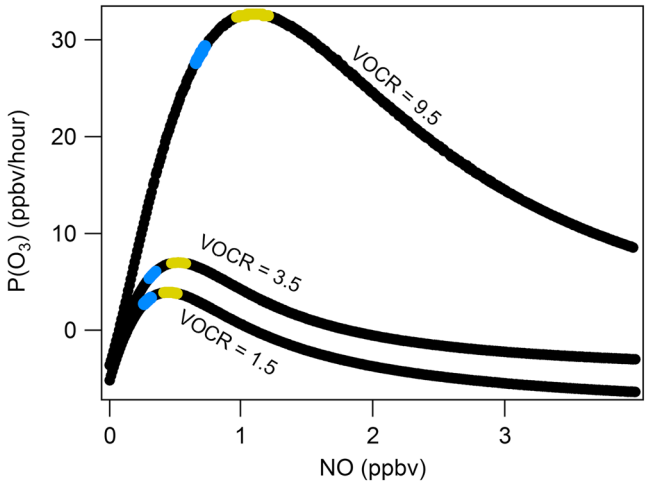

Figure 1. Curves showing $P(O_3)$ versus NO at lines of constant VOCR. Blue points highlight a LRO_x/LNO_x ratio of 1 (range 0.9–1.1) for each constant-VOC curve, and gold points highlight a ratio of 0.35 (range 0.25–0.45).

3. Results

3.1. Reevaluation of LRO_x/LNO_x as an Indicator of $P(O_3)$ Sensitivity

Two separate model simulations were run to evaluate the ability of the LRO_x/LNO_x ratio to diagnose the chemical sensitivity of $P(O_3)$ under clear-sky conditions at midday. In the first simulation, three different VOC groupings were created, corresponding to low, medium, and high VOCRs (1.5, 3.5, and 9.5 s^{-1}, respectively). Each VOC group was run 400 times, with NO varying in each run by an increment of 10 pptv, with a range of 10 pptv to 4 ppbv. This allowed for evaluation of the LRO_x/LNO_x ratio with very high resolution in NO_x at three different VOC loadings. In the second simulation, NO ranged from 10 pptv to 20 ppbv with 13 stops, and VOCR varied from 0.4 to 9.5 s^{-1} at each NO value with 30 stops, effectively creating a 13×30 grid in NO-VOCR space. This second simulation allowed for evaluation of the LRO_x/LNO_x ratio over a very wide range of atmospherically relevant chemical compositions, but with lower resolution than the first simulation. In both simulations, median mixing ratios from Colorado were used to constrain NO_x and VOCs, and VOCR was adjusted by incrementally increasing/decreasing all relevant VOCs by a given percent. In all simulations, the model was not constrained by measurements of short-lived secondary oxidation products (such as CH_2O), thus allowing the modeled radical environment to change in response to changes in VOC constraints.

Figure 1 shows the calculated $P(O_3)$ values from the first simulation as a function of NO. These results show typical behavior—at very low NO values, $P(O_3)$ is very sensitive to NO mixing ratios, and increasing NO results in an increase in $P(O_3)$. As NO increases, $P(O_3)$ eventually reaches a local maximum (which is at a different NO value depending on the VOCR), beyond which further increases in NO result in a decrease in $P(O_3)$ due to radical suppression by NO_x. Figure 1 shows that for each curve, the location where $LRO_x/LNO_x = 1$ is on the left shoulder—below the maximum $P(O_3)$—while the corresponding LRO_x/LNO_x ratio at the maximum $P(O_3)$ on each curve is ~0.35. This suggests that the chemical transition point (i.e., where $LRO_x/LNO_x = 1$) does not align with the local maximum $P(O_3)$ value, and small increases in NO beyond the chemical transition point still result in increases in $P(O_3)$. Thus, there is a small window where $0.35 < LRO_x/LNO_x < 1$ where the dominant radical removal process changes from radical-radical interactions (i.e., reactions (2)–(4)) to radical-NO_x interactions (i.e., reaction (1)), but reductions in O_3 production could still be achieved by reducing NO_x instead of solely focusing on VOCs. In effect, the $P(O_3)$ turnover point relevant for planning emissions control strategies does not necessarily line up with the chemical transition point.

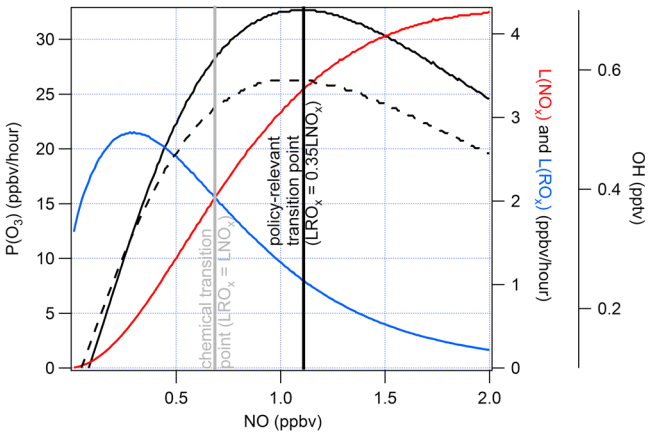

Figure 2. A plot of model-calculated values of $P(O_3)$ (solid black trace), $L(NO_x)$ (red trace), $L(RO_x)$ (blue trace), and OH (dashed black trace) over a range of NO values at a constant VOCR of 9.5 s^{-1}. The point where $L(RO_x)$ and $L(NO_x)$ are equal is marked with a vertical gray line (i.e., the chemical transition point described in *Sillman et al.* [1990]), and the maximum value of $P(O_3)$ is marked with a vertical black line (i.e., the policy-relevant turnover point).

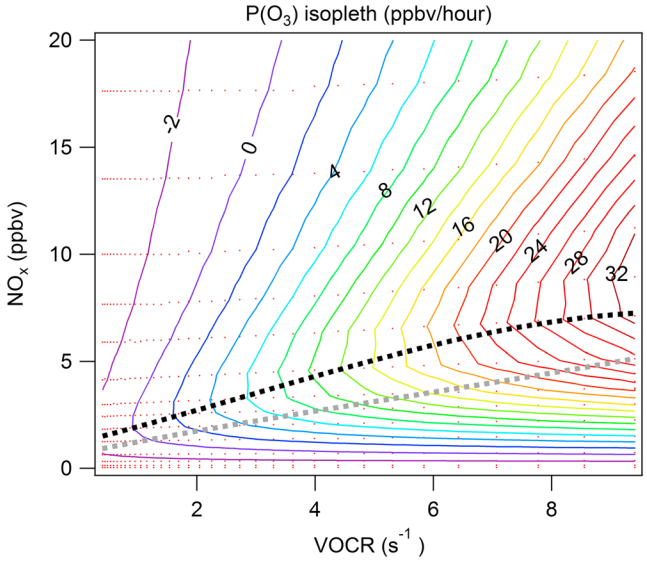

Figure 3. $P(O_3)$ isopleth, where contour lines represent constant $P(O_3)$ (with units of ppbv/h) as a function of NO and VOCR. Red dots represent the VOCR and NO compositions used as inputs to the box model. The dashed black line is a linear fit to all model runs where the LRO_x/LNO_x ratio was equal to 0.35 (range 0.25–0.45), and the dashed gray line is a linear fit to all model runs where the ratio was equal to 1 (range 0.9–1.1).

The reason for this difference is shown in Figure 2: at low NO_x loadings, the rate of LNO_x (red trace) increases as NO increases, while rate of LRO_x (blue trace) initially increases with NO, then decreases with further additions of NO. The point where these two rates are equal is marked with a gray line, while the maximum $P(O_3)$ location is marked with a black line. Although LNO_x becomes faster than LRO_x to the right of the gray line ($LRO_x/LNO_x < 1$), the ambient concentration of OH (dashed black line) increases with further increases in NO and reaches a maximum concentration concurrent with the maximum value of $P(O_3)$. Thus, even though the photochemical regime changes at the gray line (from having a dominant radical sink from radical-radical interactions to radical-NO_x interactions), $P(O_3)$ peaks at higher NO_x concentrations because the initial step in photochemical O_3 production—the oxidation of VOCs by OH—is often the rate-limiting step, and increasing NO_x increases the OH/HO_2 ratio. In effect, a smaller fraction of OH radicals react with VOC to the right of the gray line, but subsequent additions of NO_x result in growth of the available pool of OH radicals that counteracts this, and $P(O_3)$ increases. Beyond a certain point, however, further additions of NO_x result in diminishing gains or suppression of the available radical pool, and $P(O_3)$ begins to decline. This occurs because OH propagation is reduced as a larger fraction of OH radicals react with NO_2, with the system becoming strongly radical limited as NO_x continues to increase. A similar result can be seen in a publication by *Thornton et al*. [2002]; see Figure 4], where $P(O_3)$ was not at a maximum when $LRO_x/LNO_x = 1$ but rather when $LNO_x > LRO_x$. *Kleinman* [2005] further explored this topic and noted that earlier work [e.g., *Sillman et al*., 1990; *Kleinman*, 1994] made the assumption that long-lived NO_z species ($NO_z \equiv NO_y - NO_x$) such as PAN were in steady state and their net effect on the radical budget was negligible. However, *Kleinman* [2005] noted that in the presence of relatively fresh emissions, PAN is not in steady state and that when PAN was accounted for the $P(O_3)$ turnover point often occurred at $LRO_x/LNO_x < 1$. With the inclusion of alkyl nitrates—a relatively stable by-product of the reaction between RO_2 and NO—we find that the LRO_x/LNO_x ratio at the $P(O_3)$ transition point is about 0.35.

Figure 3 shows results from the second box model simulation and further expands on the idea that the chemical transition point and the policy-relevant $P(O_3)$ turnover point are not the same. In Figure 3, the model-calculated $P(O_3)$ values from the second simulation were used to create a $P(O_3)$ isopleth. Here the gray line represents a linear fit applied to all model simulations that had LRO_x/LNO_x ratios of 1 (range 0.9–1.1), and the black line represents a linear fit to all model simulations that had ratios of 0.35 (range 0.25–0.45). The general features of O_3 isopleths are noted here: moving toward the bottom and right sides of the isopleth, the chemical regime becomes increasingly NO_x limited, and reductions in NO_x would be the most effective strategy to reduce local O_3 production. Moving toward the top of the isopleth, the chemical regime becomes increasingly radical limited, and decreasing emissions of VOCs would be the most effective strategy to reduce local O_3 production, while minor reductions in NO_x emissions could potentially increase local O_3 production. One caveat, however, is that the effectiveness of reducing anthropogenic VOC emissions relative to reducing NO_x emissions will depend on the level of natural VOC emissions in a given region. In Figure 3, the black line represents the actual $P(O_3)$ turnover point better than the gray line. Because the primary goal of this work is

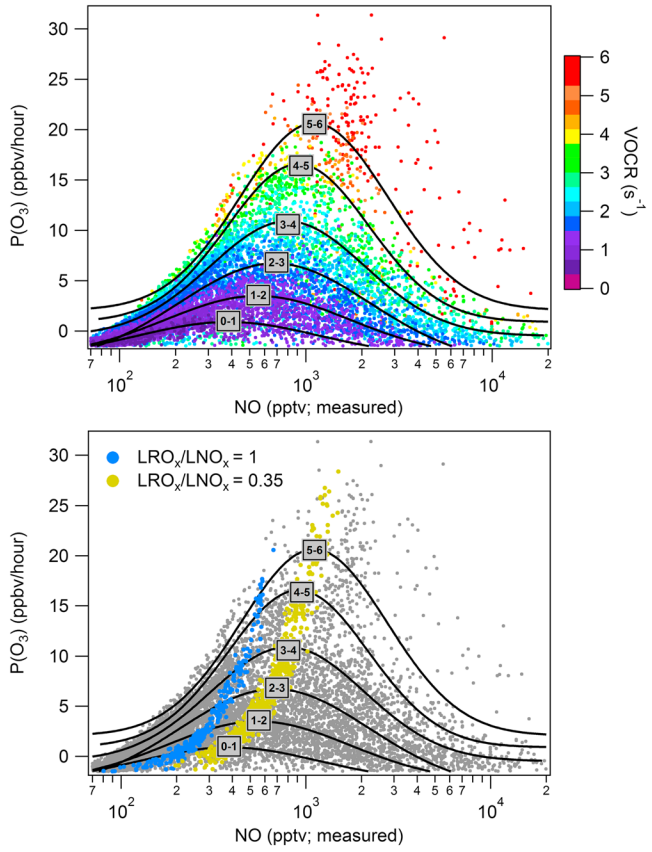

Figure 4. Similar to Figure 1, except showing model calculations based on field measurements from Colorado. (top) $P(O_3)$ versus NO, colored by VOCR, where black lines represent lognormal fits for data that fall within the VOCR range specified by text boxes. For example, the black line that intersects the text box that reads "3-4" is the lognormal fit of all data that had VOCR between 3 and 4. (bottom) Points with a LRO_x/LNO_x ratio of 1 (0.9–1.1) are highlighted blue, and points with a LRO_x/LNO_x ratio of 0.35 (0.25–0.45) are highlighted gold. The position of the text boxes is the same in each panel.

to develop a tool for assessing $P(O_3)$ sensitivity from space, a LRO_x/LNO_x ratio of 0.35 will be used to indicate the $P(O_3)$ sensitivity transition point.

While the simulations presented above are useful for determining the relationship between LRO_x/LNO_x and $P(O_3)$ from a theoretical standpoint, field data are more useful for exploring this relationship within a realistic range space of temperatures, pressures, solar intensities, and chemical compositions. Figure 4 shows results from model simulations constrained by in situ aircraft measurements from the Colorado deployment of DISCOVER-AQ. The broad range of NO, VOCR, and $P(O_3)$ spanned by the data provide an excellent set of observations for exploring the behavior of the CH_2O/NO_2 ratio in relation to the O_3 photochemical controls. Figure 4 (top) shows model-calculated $P(O_3)$ versus measured NO, colored by VOCR. The numbered text boxes indicate the $P(O_3)$ sensitivity transition point (or local $P(O_3)$ maximum) for the specified VOCR range, which was calculated by fitting the data from within the specified VOCR range to a lognormal fit (shown as solid black traces) and finding the point where the first derivative was equal to 0. For example, the box labeled "4-5" represents the inflection point of the lognormal $P(O_3)$ curve when only data with VOCR between 4 and 5 were considered. The bottom panel shows this same plot, colored such that a LRO_x/LNO_x ratio of 1 appears blue, and a LRO_x/LNO_x ratio of 0.35 appears gold (the text box labels are in the same position). Here it is clear that using a LRO_x/LNO_x ratio of 0.35 better represents the actual transition point (i.e., it lines up with the text boxes), while using a LRO_x/LNO_x ratio of 1 tends to overstate the "radical-limited nature" of these data. Next, the effectiveness of the CH_2O/NO_2 ratio as an indicator of the local photochemical regime and $P(O_3)$ sensitivity will be explored and tested against the LRO_x/LNO_x ratio.

3.2. CH_2O/NO_2 and Its Relationship With LRO_x/LNO_x and $P(O_3)$

To quantify variability in the correlation between CH_2O/NO_2 and LRO_x/LNO_x, a similar approach to that of *Duncan et al.* [2010] was applied to data collected from the Colorado deployment of DISCOVER-AQ. The Colorado data set is of special interest here because nearly half of the column CH_2O/NO_2 ratios measured there fall in the range 0–2 (i.e., radical limited or in the transition/ambiguous range identified in *Duncan et al.* [2010], likely because of low biogenic VOC emissions). Figure 5 shows distributions of the column CH_2O/NO_2 ratios measured during each DISCOVER-AQ deployment. In Maryland and Houston, only 12% and 25% of the column CH_2O/NO_2 ratios fall in the range 0–2, implying that both were predominantly NO_x limited during their respective campaigns. More than 70% of the column CH_2O/NO_2 ratios measured in California fall within the range 0–2, but the average CH_2O column density in California was 0.14 DU

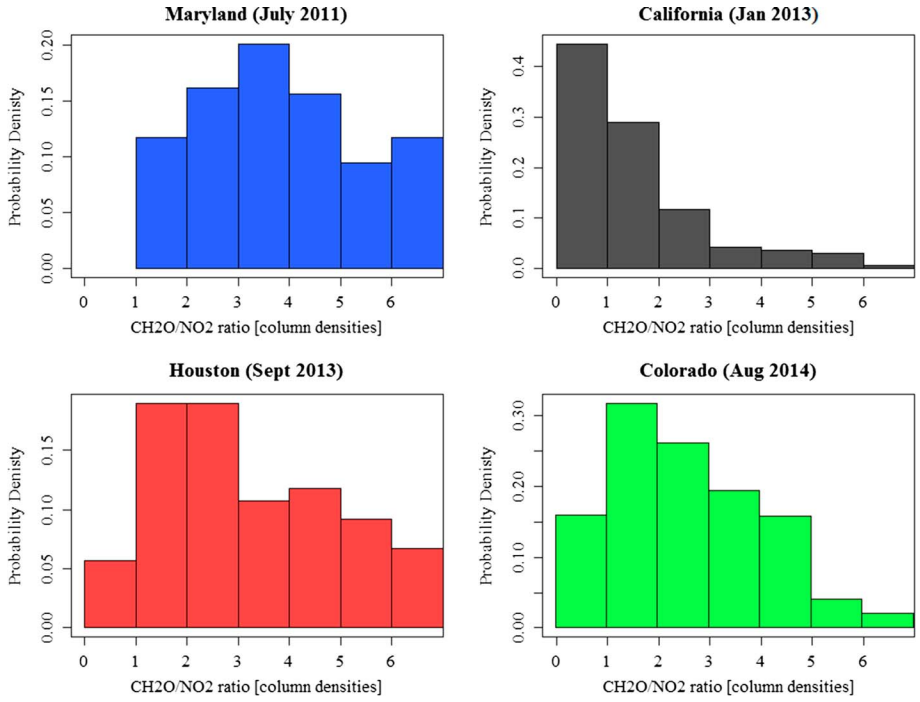

Figure 5. Histograms showing the distribution of column CH_2O/NO_2 ratios for each DISCOVER-AQ location.

(Dobson unit or 2.69×10^{16} molecules cm^{-2}). This is well below the anticipated CH_2O sensitivity of ~0.3 DU expected from TEMPO. It should be noted, however, that the wintertime deployment of DISCOVER-AQ-California was focused on aerosol events rather than O_3 photochemistry. Therefore, the Colorado data set provides the best opportunity to evaluate the relationship between CH_2O/NO_2 and LRO_x/LNO_x in radical-limited regimes, NO_x-limited regimes, and in the transition/ambiguous range. Additionally, the FRAPPE field campaign extensively studied air pollution and photochemistry in the Northern Front Range area at the same time as the DISCOVER-AQ-Colorado deployment, meaning that the VOC mapping technique that we use to derive inputs for box model simulations (described in detail in *Schroeder et al*. [2016]) is the most robust in Colorado.

Using model-calculated values of LRO_x/LNO_x and in situ measurements of CH_2O and NO_2, we find, like *Tonnesen and Dennis* [2000] and *Duncan et al*. [2010], that a range of CH_2O/NO_2 ratios are associated with the previously described $P(O_3)$ sensitivity transition point (i.e., where $LRO_x/LNO_x = 0.35$). Figure 6 shows plots of measured CH_2O/NO_2 and NO_2 as functions of model-predicted LRO_x/LNO_x in Colorado, Houston, and Maryland. In Colorado, we found a range $0.9 < CH_2O/NO_2 < 1.8$ that lies in the transition/ambiguous region, whereas Houston had a range $0.7 < CH_2O/NO_2 < 2.0$ and Maryland had a range $1.0 < CH_2O/NO_2 < 2.3$. Because we used a LRO_x/LNO_x ratio of 0.35 instead of 1 as a cutoff, our associated ranges of CH_2O/NO_2 values are expected to be slightly different than the range described in *Duncan et al*. [2010]. Additionally, *Duncan et al*. [2010] focused on Southern California, whereas we show data from Colorado, Houston, and Maryland, with differences in the CH_2O/NO_2 transition/ambiguous range between the three locations indicating regional variability in the transition/ambiguous range of CH_2O/NO_2. *Duncan et al*. [2010] also looked at low-resolution 3-D model outputs (36×36 km^2) over the continental U.S. and identified a CH_2O/NO_2 transition/ambiguous range of 1.5–2.5, although they note that low-resolution modeling may effectively dilute gradients in NO_2. Interestingly, NO_2 (red traces in Figure 6) also displays a strong relationship with LRO_x/LNO_x, suggesting that NO_2 alone could be used as an indicator for O_3 sensitivity. This is essentially due to the fact that variations in NO_2 make a much greater contribution to variations in the ratio than does CH_2O.

At the LRO_x/LNO_x transition point (vertical blue line) in the Colorado data, CH_2O/NO_2 has values within the range 1.3 ± 0.4 (1σ, relative standard deviation = 30%), which encompasses 16% of the data, while NO_2

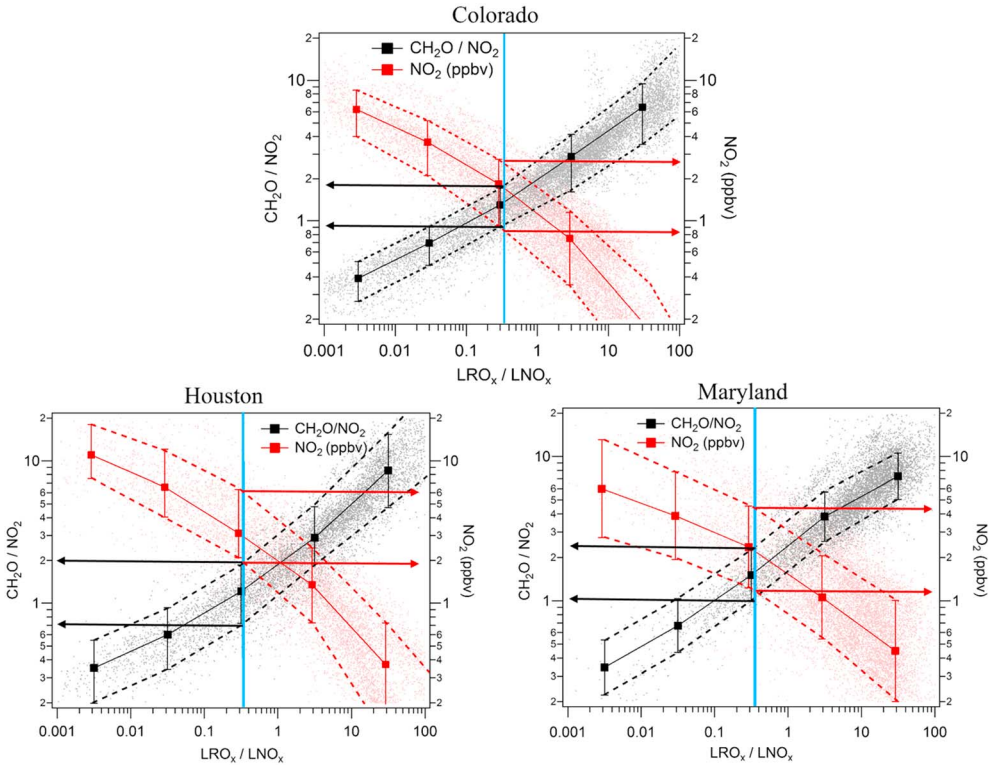

Figure 6. Plots of the model-calculated LRO_x/LNO_x ratio versus the in situ CH_2O/NO_2 ratio (black) and versus NO_2 (red) for in situ data collected in the Colorado, Houston, and Maryland deployments of DISCOVER-AQ. The solid blue line represents a LRO_x/LNO_x ratio of 0.35. For both the CH_2O/NO_2 and NO_2 data, binned averages were calculated (shown as squares), and the standard deviation for each bin is shown as error bars on each square. The dashed black and red lines connect the standard deviations between each binned point.

has values within the range 1.83 ± 0.95 ppbv (1σ, 52% relative standard deviation) and encompasses 30% of the data. Although the uncertainty range associated with NO_2 is larger, the possibility of using it as a sole indicator of O_3 sensitivity is intriguing nonetheless and could have merit in certain environments. For example, in regions with low CH_2O (such as Colorado, where many of the aircraft column densities lie near the anticipated TEMPO sensitivity for CH_2O), NO_2 may be the best available option for examining O_3 sensitivity from space. In Houston and Maryland, the NO_2 values that define the transition/ambiguous region were 4.0 ± 1.8 (1σ, 50% relative standard deviation) and 2.8 ± 1.5 (1σ, 54% relative standard deviation), respectively. Additionally, because biogenic emissions vary greatly between regions and throughout the year, location and season-specific NO_2 transition/ambiguous ranges would have to be determined to account for this. On the other hand, ambient CH_2O changes in response to biogenic emissions and the CH_2O/NO_2 ratio will change in accordance. Thus, CH_2O/NO_2 makes a more useful indicator of O_3 sensitivity than simply using NO_2 because fewer data points fall into the transition/ambiguous region, and the CH_2O/NO_2 ratio will change in response to changes in emissions of both NO_x and/or VOCs.

As described in *Tonnesen and Dennis* [2000] and *Duncan et al.* [2010], there is a large degree of uncertainty in choosing an actual transition point within the CH_2O/NO_2 range. *Tonnesen and Dennis* [2000] found that CH_2O/NO_2 ratios in the range 0.8–1.8 lie in the transition/ambiguous region, and *Duncan et al.* [2010] found that ratios falling in the range 1.0–2.0 are in the transition/ambiguous region. This range of values can be attributed to the fact that CH_2O and NO_2 are used as proxies for radical production and NO_x loadings, respectively, but their relationships are not linear with these quantities over wide ranges of conditions. For example, CH_2O, while considered relatively short lived ($\tau \approx 1$–3 h at midday), has a lifetime that is orders of magnitude longer than most radical species. Thus, if a large pulse of NO_x or VOC emissions were introduced to an air mass, radical species and NO_x partitioning would reach new steady state concentrations within minutes,

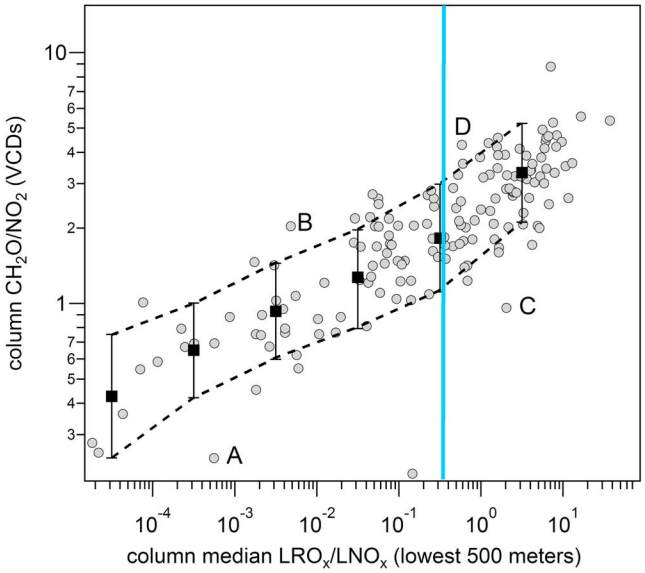

Figure 7. The ability of the lower tropospheric column CH_2O/NO_2 ratio (from P-3B integrated vertical column densities (VCDs) in Colorado) to act as a proxy for near-surface LRO_x/LNO_x. Near-surface LRO_x/LNO_x is represented as the median of the bottom 500 m of each spiral. Gray circles represent each spiral conducted in Colorado, and black squares represent the binned average and standard deviation of column CH_2O/NO_2. The blue line represents the O_3 sensitivity turnover point at $LRO_x/LNO_x = 0.35$. The blue line crosses the binned CH_2O/NO_2 standard deviation bars at CH_2O/NO_2 values of 1.1 and 3.0. Vertical profiles of CH_2O and NO_2 for select spirals (tagged as A, B, C, and D) are shown in the supporting information.

while CH_2O would be slower to respond and the ability of CH_2O to act as a proxy for radicals would be temporarily diminished until it reaches its new steady state concentration. NO_x also affects the relative production rates of RO_2 and CH_2O, leading to variability in the correlation between CH_2O and radical production. *Wolfe et al.* [2016] found that on average, the production rates of CH_2O and RO_2 in the southeast U.S. both increased with increasing NO_x, but there was substantially more variability in the RO_2 response to increases in NO_x. Because individual VOCs have different relative branching ratios for radical and CH_2O formation, regions with spatially inhomogeneous VOC compositions will have different relationships between CH_2O and radicals and different responses to changes in NO_x. Additionally, the two primary sinks of CH_2O (photolysis and reaction with OH) have varying rates, with the two being nearly equal in high OH environments and photolysis dominating in low OH environments [*Valin et al.*, 2015]. So modulations in ambient OH concentrations in response to NO_x also affect the relationship between ambient CH_2O and radicals by increasing the rates of CH_2O and radical formation but decreasing the CH_2O lifetime. Finally, reactions between O_3, water vapor, and sunlight act as a primary radical source (via OH formation), which can make up a substantial portion of total radical production in some environments. This implies that both O_3 and water vapor may also affect the ability of CH_2O and NO_2 to act as indicator species [*Sillman and He*, 2002; *Tonnesen and Dennis*, 2000]. To summarize, in environments with diverse VOC compositions and wide ranges of NO_x loadings, O_3 mixing ratios, and humidities, the correlation between CH_2O/NO_2 and LRO_x/LNO_x is less distinct, and a single CH_2O/NO_2 ratio may not represent the $P(O_3)$ sensitivity transition point over all ranges of conditions. Additionally, because the relative importance of individual factors varies regionally, we see regional differences in the range of CH_2O/NO_2 values that indicate the transition/ambiguous range between NO_x- and radical-limited environments. Disentangling the role that each of the factors described above plays on the relationship between LRO_x/LNO_x and CH_2O/NO_2 would make for an interesting follow-up study but is beyond the scope of the work presented here.

3.3. Application to CH_2O/NO_2 Column Densities

The previous section showed that a wide range of CH_2O/NO_2 ratios fall within the transition/ambiguous range, with variability in the range of transition/ambiguous values between regions. However, the previous section (and previous work by *Tonnesen and Dennis* [2000] and *Duncan et al.* [2010]) used high-frequency in situ data to explore this relationship, and the primary goal of this study is to evaluate the ability of satellite-based measurements of CH_2O/NO_2 to diagnose near-surface $P(O_3)$ sensitivity. The unique data set and statistics provided by DISCOVER-AQ allows for the first evaluation of this relationship in the context of satellite measurements without significant input from global models, enabling us to expand upon the results of *Duncan et al.* [2010]. In this section, the relationships observed in the previous section are evaluated in the context of column densities derived from profile measurements in Colorado. Figure 7 shows a similar plot to Figure 6—except that CH_2O and NO_2 aircraft column densities are used instead of mixing ratios, and $LRO_x/$

LNO_x was taken as the median value from the lowest 500 m of each spiral. Surface measurements at each spiral site were not extensive enough to allow for calculation of LRO_x/LNO_x at the surface, so the median value from the bottom 500 m of each spiral is our best approximation of near-surface conditions. Similar trends are noted here: low column CH_2O/NO_2 ratios tend to correlate with low near-surface LRO_x/LNO_x ratios, and vice versa. However, when the near-surface LRO_x/LNO_x ratio was near the transition point ($LRO_x/LNO_x = 0.35$), a range of column CH_2O/NO_2 values was observed. When in situ data from Colorado were used (as in Figure 6), CH_2O/NO_2 ratios in the range 0.9–1.8 were found to coincide with a LRO_x/LNO_x ratio of 0.35, whereas when column densities were used (as in Figure 7), column CH_2O/NO_2 ratios in the range 1.1–3.0 coincided with a near-surface LRO_x/LNO_x ratio of 0.35. Using the approach of *Martin* [2004], who used a distinct CH_2O/NO_2 ratio of 1 as the transition point, we would classify 16% of DISCOVER-AQ-Colorado spirals as radical limited and 84% as NO_x limited. Using the approach of *Duncan et al.* [2010], who defined the column transition/ambiguous region as $1 < CH_2O/NO_2 < 2$, we would classify 16% of spirals as radical limited, 32% as transition/ambiguous, and 52% as NO_x limited. Using the transition/ambiguous range that we report here for Colorado ($1.1 < CH_2O/NO_2 < 3.0$), we would classify 19% of spirals as radical limited, 53% as transition/ambiguous, and 28% as NO_x limited. These differences could have broad implications for policymakers looking to use satellites to aid in reducing emissions of O_3 precursors, as we find that for more than half of the Colorado data, reductions in both VOCs and NO_x would be the best strategy for reducing O_3 production.

When column densities are used instead of in situ measurements, the low end of the transition/ambiguous range increased from 0.9 to 1.1, and the upper end of the range increased from 1.8 to 3.0. The upward shift in the low end of the range is likely because of subtle differences in the vertical distributions of CH_2O and NO_2. Figure 8 shows median vertical profiles of CH_2O and NO_2 from Colorado. Both CH_2O and NO_2 are reasonably well mixed on average in the lowest 500 m, but above that altitude, NO_2 decreases more rapidly compared to CH_2O. This could be due in part to the in situ production of CH_2O throughout the planetary boundary layer (PBL, the lowest portion of the vertical column that is chemically perturbed by surface emissions, typically extending 1–3 km above the surface) while NO_2 must be vertically mixed from the surface. Another factor would be the change in NO_x partitioning with altitude as lower temperatures lead to more NO in relation to NO_2. In the lower free troposphere, CH_2O has a nonnegligible presence that extends to the top of the profiles, while NO_2 mixing ratios are negligible above 3 km. Therefore, the column CH_2O/NO_2 ratio will have a slightly higher value than a colocated in situ CH_2O/NO_2 ratio near the surface, and the column CH_2O/NO_2 ratios shown in Figure 7 are slightly offset relative to the in situ CH_2O/NO_2 ratios shown in Figure 6. Furthermore, when using column CH_2O/NO_2 ratios to estimate near-surface conditions, additional uncertainties are created by nonuniform mixing in the lower troposphere. That is, changes in surface mixing ratios of CH_2O and NO_2 may be decoupled from changes in column densities, and concurrent changes in surface mixing ratios and column densities may not be proportional [*Fishman et al.*, 2008; *Flynn et al.*, 2014]. Select spirals (tagged as A, B, C, and D in Figure 7) demonstrate this and are shown in the supporting information. In spiral A, collected at midday over the Denver-La Casa site, there is a large spike in NO_2 (in excess of 30 ppbv) at ~2.5 km (~1 km above the bottom of the spiral), with no concurrent spike in CH_2O. Because this spike was not located near the surface, the column NO_2 value for this spiral was higher than the mixing ratio near the surface, and the column CH_2O/NO_2 ratio was lower than what one would expect given the near-surface LRO_x/LNO_x ratio. In spiral B, collected in the morning over the National Renewable Energy Laboratory-Golden site, there was an anomolously high amount of CH_2O in the free troposphere—about 1 ppbv all the way up to an altitude of 4.5 km, with negligible presence of NO_2 above the PBL. Here the column CH_2O/NO_2 was higher than one would expect from the near-surface LRO_x/LNO_x ratio. Spiral C is similar to spiral A, in that there was a large spike in NO_2 above the surface that was decoupled from any change in CH_2O. Here like spiral A, the column CH_2O/NO_2 was lower than one would expect given the near-surface LRO_x/LNO_x ratio. In spiral D, CH_2O decreased sharply toward the bottom of the spiral, while NO_2 stayed fairly constant. In this case, the CH_2O/NO_2 ratio at the very bottom of the spiral was lower than in the rest of the PBL, so the column CH_2O/NO_2 ratio was not indicative of near-surface conditions. These four spirals were chosen to demonstrate to readers how anomalies in the free tropospheric CH_2O contribution and inhomogeneities in the lower tropospheric mixing can create a larger degree of uncertainty, and therefore a larger apparent transition/ambiguous range, when using column CH_2O/NO_2 as an indicator of near-

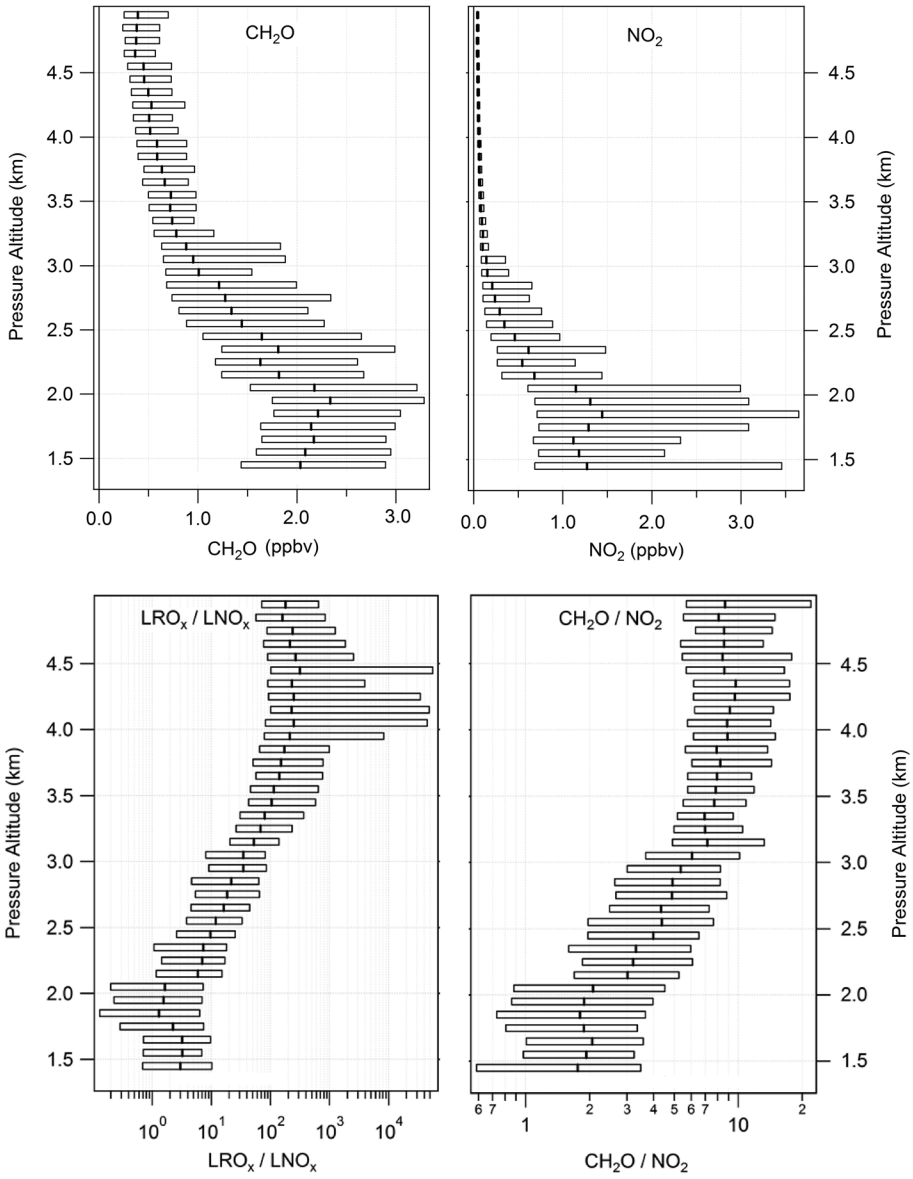

Figure 8. Binned statistics for vertical profiles of CH_2O, NO_2, LRO_x/LNO_x, and CH_2O/NO_2 from Colorado. All data were binned every 100 m, and the median, 25th percentile, and 75th percentile for each bin are shown.

surface O_3 sensitivity. However, the environment yielding these results must be placed in context: these data were collected primarily during fair weather periods (clear or partly cloudy) during 1 month, and extrapolation of these results to other meteorological conditions, seasons, and years may not be appropriate. Changes in cloud cover as well as seasonal variations in temperature and humidity could affect vertical mixing, secondary CH_2O production, and the lifetimes of NO_x and CH_2O, potentially changing the chemistry and distribution of these species in the atmosphere. Additionally, seasonal variations in long-range transport and varying emission strengths of far-field upwind sources (such as wildfires) along with interannual variability in synoptic-scale meteorological conditions may also affect the chemistry and vertical distribution of CH_2O and NO_2 in the atmosphere. Therefore, caution must be used when trying to extrapolate these results to different conditions.

Similar calculations to those performed for Colorado were also performed to evaluate the ability of column CH_2O/NO_2 to indicate near-surface O_3 sensitivity in Houston and Maryland. Plots of the column CH_2O/NO_2 ratio for each spiral as a function of the near-surface LRO_x/LNO_x ratio from these two DISCOVER-AQ

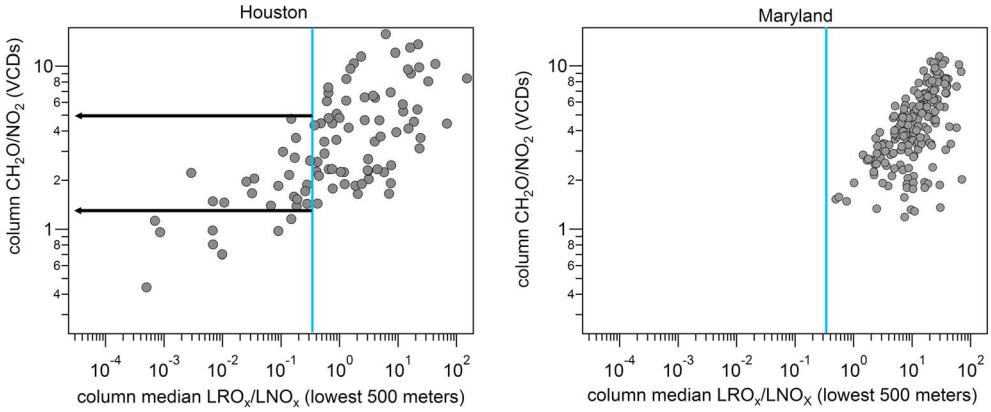

Figure 9. Similar to Figure 7, except with data from Houston and Maryland. Note that the scales are the same for these two plots, but the *x* axes are different than in Figure 7.

deployments are shown in Figure 9. In Houston, we find a transition/ambiguous range of $1.3 < CH_2O/NO_2 < 5.0$, while in Maryland, we find that all of the spirals fell above the LRO_x/LNO_x transition point. Therefore, further analysis cannot be performed on the Maryland data set, as it is entirely NO_x limited when viewed in this context. With respect to the Houston data, if one were to apply a CH_2O/NO_2 ratio of 1 as a distinct transition point (as in *Martin* [2004]), 5% of the Houston spirals would be classified as radical limited, with the rest being NO_x limited. If we define the transition/ambiguous range as $1 < CH_2O/NO_2 < 2$ (as in *Duncan et al.* [2010]), we would classify 5% of the spirals as radical limited, 20% as transition/ambiguous, and 75% as NO_x limited. Using the uncertainty range that we derive here ($1.3 < CH_2O/NO_2 < 5.0$), we classify 9% of the spirals as being radical limited, 56% as transition/ambiguous, and 35% as NO_x limited. Similar to our results from Colorado, the larger range of uncertainty in the column CH_2O/NO_2 ratio that we note in Houston increases the number of spirals that are labeled as transition/ambiguous and could affect emission reduction strategies derived from satellite measurements of CH_2O/NO_2.

4. Temporal Evolution of $P(O_3)$ Sensitivity

In section 1, we briefly described how the low spatial resolution of present-day low Earth-orbiting instruments (such as OMI) often necessitates long-term averaging to resolve spatial gradients. This long-term averaging, however, masks any temporal gradients that may exist within the averaging period. One must consider the possibility that photochemical conditions on O_3 exceedance days may be different from those on nonexceedance days, and the CH_2O/NO_2 ratios and O_3 sensitivities derived from long-term averaging may include a mix of exceedance and nonexceedance days. In section 4.1, we use data from DISCOVER-AQ-Houston to demonstrate additional information that can be gained by high-frequency monitoring of the temporal evolution of the column CH_2O/NO_2 ratio and consider the additional information that future geostationary orbiting satellites, such as TEMPO, may provide in the context of diagnosing O_3 sensitivity on exceedance days versus nonexceedance days. However, because of the uncertainty in satellite retrievals of CH_2O and NO_2, long-term averaging of TEMPO data may still be desired to better resolve spatial gradients in certain environments. However, because TEMPO will provide multiple viewings each day, long-term averaging of data from distinct times of day may provide additional information about diurnal tendencies in O_3 sensitivity that are not possible with current instruments such as OMI. In section 4.2, we use DISCOVER-AQ data from Colorado and Houston to calculate long-term averages of the column CH_2O/NO_2 ratio at morning, midday, and afternoon to provide a preview of how TEMPO may allow researchers to view the diurnal evolution of local photochemical environments in the aggregate.

4.1. Continuous Monitoring of Column CH_2O/NO_2: Diagnosing Differences in the Photochemical Environment on O_3 Exceedance Days Versus Nonexceedance Days

Much of the DISCOVER-AQ-Houston deployment was characterized by persistently low O_3, and no O_3 exceedances were recorded until the research flight on 25 September 2013. On this day, the sky was clear and

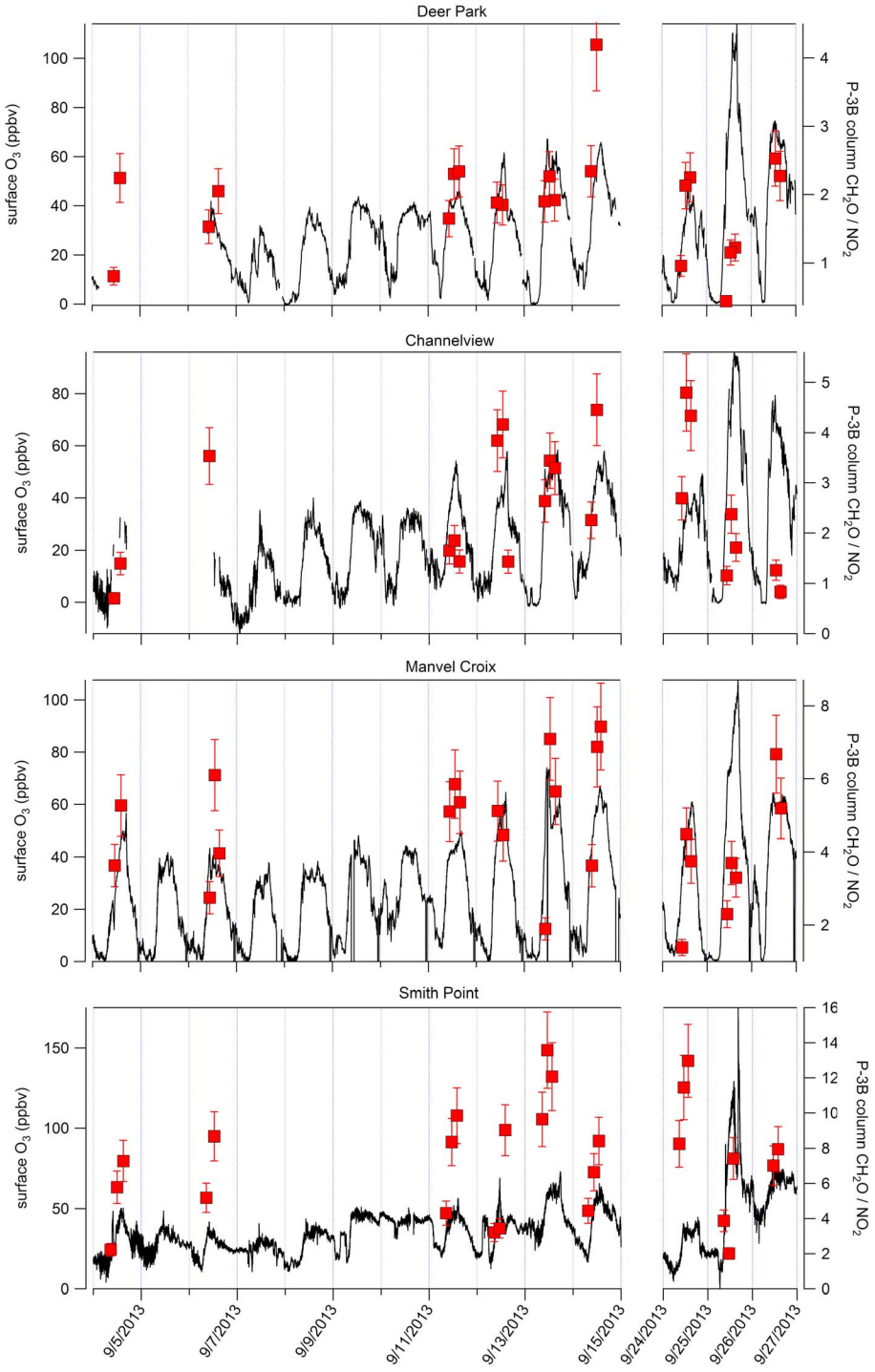

Figure 10. Surface O_3 (black trace, left axis) and aircraft column CH_2O/NO_2 ratios (red squares, right axis, ±15% uncertainty) from four sites in Houston during DISCOVER-AQ. The days 15 to 23 September 2013 are omitted for clarity, as no flights were flown on these days.

conditions were hot and fairly stagnant. Previous research has also indicated that anthropogenic emissions from the ship channel area may have been stronger than on other days [*Fried et al.*, 2016]. Under these conditions, O_3 production was high and O_3 mixing ratios in excess of 100 ppbv were observed throughout the region, with a maximum of 145 ppbv measured south of downtown Houston. Because this extreme exceedance day was preceded by many nonexceedance days, DISCOVER-AQ-Houston represents a near-

Table 1. The Average Midday Aircraft Column CH_2O/NO_2 Ratio (Taken as Average From Every Flight Day, ±1 Standard Deviation) and the Aircraft Column CH_2O/NO_2 Ratio From Morning, Midday, and Afternoon From Four Sites in Houston on 25 September[a]

Location	DISCOVER-AQ Midday Average of Column CH_2O/NO_2	Column CH_2O/NO_2 on 25 September		
		Morning	Midday	Afternoon
Deer Park	2.3 ± 0.8	0.4	1.1	1.2
Channelview	3.0 ± 1.4	1.1	2.4	1.7
Manvel Croix	5.7 ± 1.3	2.2	3.7	3.3
Smith Point	7.6 ± 3.3	3.9	2.0	7.4

[a]Because DISCOVER-AQ flights predominantly took place during clear-sky and partly cloudy conditions, the midday average column CH_2O/NO_2 meant to approximate monthly averages obtained from a low Earth-orbiting platform such as OMI.

ideal case study to evaluate any discrepancies between long-term averaging and high-resolution monitoring of column CH_2O/NO_2 ratios.

Figure 10 shows continuous surface O_3 measurements from four sites in Houston during the DISCOVER-AQ period, along with aircraft column CH_2O/NO_2 ratios from days where the P-3B flew. Here the extreme O_3 event of 25 September can clearly be seen in the surface O_3 monitors, and column CH_2O/NO_2 ratios at all four sites tended to be lower on 25 September than on the rest of the campaign. These results are quantitatively shown in Table 1, which compares the average column CH_2O/NO_2 ratio from all midday spirals at each site during DISCOVER-AQ to morning, midday, and afternoon spirals on 25 September. Because DISCOVER-AQ flights predominantly flew during fair weather conditions, the average midday CH_2O/NO_2 ratio that we show is analogous to what would be provided from long-term averaging of data from an instrument in low Earth orbit, such as OMI (although it should be noted that the diameter of our spirals was substantially less than the pixel width provided by OMI, so this is not meant to be a direct comparison). Given the transition/ambiguous range that we observed in Houston ($1.3 < CH_2O/NO_2 < 5.0$; see section 3.3), long-term averaging of the two sites near the ship channel (Deer Park and Channelview) would lead to their classification as transition/ambiguous, while long-term averaging would lead to Manvel Croix and Smith Point being classified as NO_x limited. On 25 September, however, Deer Park started off with a low CH_2O/NO_2 ratio in the morning (0.7, which is radical limited, compared to a midday average of 2.3, which is in the transition/ambiguous region) and rose to 1.1 and 1.2 by midday and afternoon, respectively. Based on this, Deer Park would be classified as radical limited throughout the day on 25 September, in disagreement with the result provided by long-term averaging. A similar result is noted at Channelview, Manvel Croix, and Smith point as well—column CH_2O/NO_2 ratios on 25 September at these three sites were lower than their respective long-term averages. Long-term averaging at Channelview yields a ratio of 3.0, leading to its classification as transition/ambiguous, while on 25 September, Channelview began the day in the radical-limited regime before entering into the transition/ambiguous regime for the rest of the day (albeit with a lower CH_2O/NO_2 ratio than the long-term average). However, it should be noted that the CH_2O/NO_2 ratio at Channelview at midday on 25 September is within the stated standard deviation from its monthly average, so photochemical conditions at Channelview on 25 September may not have been statistically different from the monthly average. Long-term averaging would lead to both Manvel Croix and Smith Point being classified as NO_x limited (average CH_2O/NO_2 ratios of 5.7 and 7.6, respectively), but Manvel Croix was in the transition/ambiguous region all day on 25 September, and Smith Point was in the transition/ambiguous region in morning and midday, before becoming NO_x limited again in the afternoon.

This case study serves to highlight one of the potential ways in which geostationary satellites may provide air quality planners with useful information beyond what could be provided by instruments such as OMI. The improved spatial resolution of TEMPO will mean that long-term averaging may not be required to reduce effective pixel size and achieve relevant spatial resolution. In this case study, O_3 mitigation strategies that are based on data obtained from long-term averages could lead one to conclude that reductions in NO_x would be sufficient to reduce O_3 production in Houston. However, in this case study, the best course of action to reduce O_3 on 25 September would have been to reduce emissions of both NO_x and VOCs. Clearly, a change in the overall photochemical environment of the greater Houston area from NO_x limited toward transition/ambiguous or radical limited had a large impact on regional O_3 production.

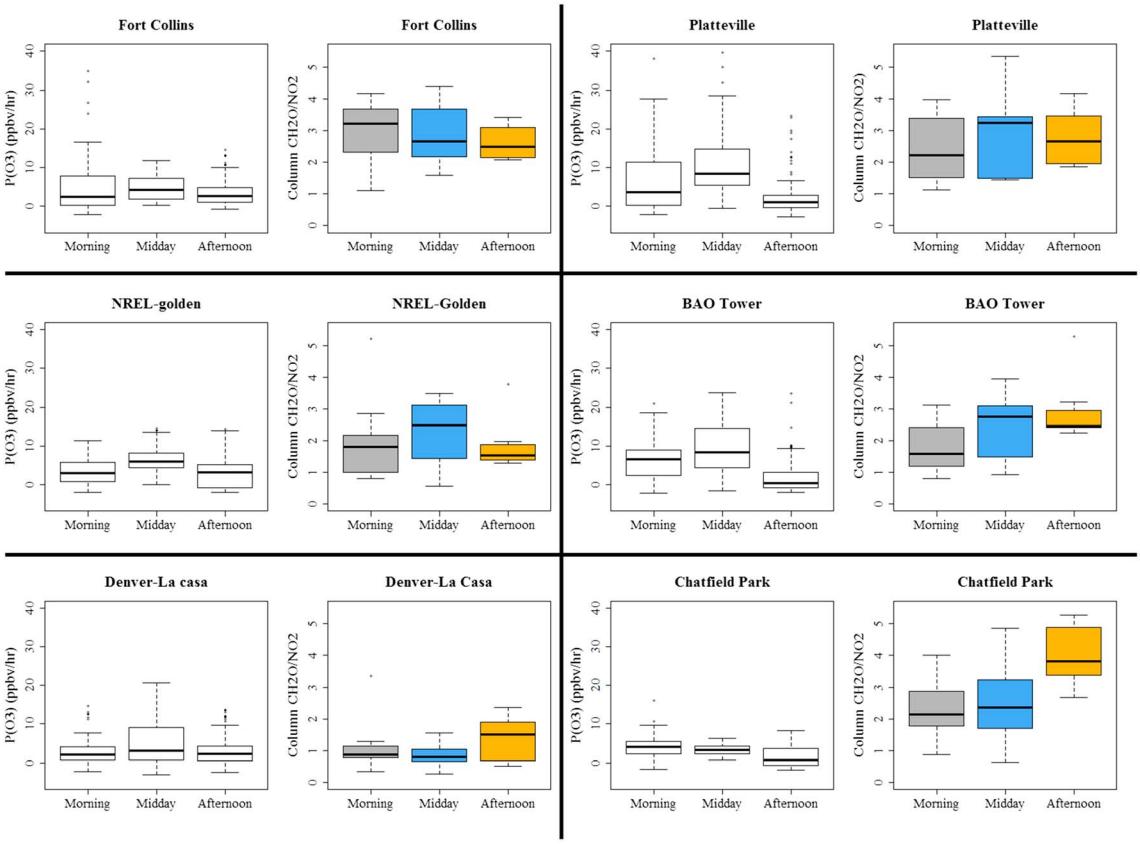

Figure 11. Box and whisker plots showing the median, 25th percentile, and 75th percentile of aircraft column CH_2O/NO_2 ratios and near-surface $P(O_3)$ (below 1 km) from each spiral site in Colorado, binned by time of day. Here morning is defined as before 11:00 local time, midday as 11:00–13:30, and afternoon as after 13:30. The dashed horizontal lines represent the upper and lower limits of the column-based transition/ambiguous region (described in section 3.3 as spanning the range 1.1–3.0 in Colorado).

4.2. Long-Term Averages of Column CH_2O/NO_2 at Distinct Times of Day

Long-term averaging of OMI retrievals provides an aggregate view of local photochemical environments around midday, while long-term averaging of TEMPO retrievals will allow researchers to view aggregate photochemical conditions at multiple times of day. As discussed in section 1, the sensitivity of the MDA8 O_3 to changes in VOC and NO_x precursor emissions is determined by the cumulative production of O_3 and NO_2 over the course of the day, and photochemical conditions often change from radical limited in the early morning to NO_x limited as the day progresses [*Tonnesen and Dennis*, 2000]. As shown in section 3, aircraft column CH_2O/NO_2 measurements from Colorado and Houston indicate that the photochemical environment in much of these regions lie in the transition/ambiguous region, while Maryland was almost entirely NO_x limited. Therefore, this section will use aircraft spirals from the Colorado and Houston deployments of DISCOVER-AQ to explore the potential utility of geostationary instruments, such as TEMPO, in observing diurnal tendencies of near-surface O_3 sensitivity from space.

Figure 11 shows campaign average statistics of aircraft column CH_2O/NO_2 at morning (gray), midday (blue), and afternoon (gold) at each spiral site in Colorado, along with model-predicted $P(O_3)$ from within 1 km of the surface. Here much of the data lie in the transition/ambiguous region, but there are notable exceptions. In Fort Collins, the median photochemical environment is NO_x limited in the morning but falls into the transition/ambiguous region during midday and afternoon. In Platteville, most of the data lie in the transition/ambiguous region, but the median photochemical environment at midday is slightly NO_x limited. The Denver-La Casa site is the only site to feature a median photochemical condition that is radical limited, which occurred in the morning and at midday before moving to the transition/ambiguous region in the afternoon. This is in agreement with regional modeling studies that concluded that most of Colorado was NO_x

limited or near the transition/ambiguous point with the exception of the Denver urban core, which was radical limited [*Colorado Department of Public Health and Environment* (*CDPHE*), 2008]. *McDuffie et al*. [2016] used a box model constrained with surface-based observations at Boulder Atmospheric Observatory (BAO) Tower (over a time period which partially overlapped with DISCOVER-AQ-Colorado and FRAPPE) and reported that O_3 production at BAO Tower was, generally, NO_x limited. Using data from the lowest 500 m of our spirals over BAO Tower, we report an average LRO_x/LNO_x ratio of 1.9, which, in agreement with *McDuffie et al*. [2016], indicates that BAO Tower was NO_x limited. Additionally, we find that the period of highest $P(O_3)$ occurred around midday, indicating that reductions in NO_x emissions would be effective in reducing local O_3. However, because of the large transition/ambiguous region that we report for column CH_2O/NO_2 ratios in Colorado (see section 3.3, where the transition/ambiguous range was determined to be $1.1 < CH_2O/NO_2 < 3.0$), our aircraft column densities indicate that typical conditions at BAO Tower were transition/ambiguous. This serves to highlight one of the drawbacks of using column CH_2O/NO_2 as an indicator of near-surface O_3 sensitivity: regions that are anywhere near the photochemical transition point ($LRO_x/LNO_x = 0.35$) are unable to be classified as radical limited or NO_x limited. In this case, only three of the 18 boxplots in Figure 11 have median CH_2O/NO_2 values that indicate NO_x-limited conditions, while 60% of all data collected within 1 km of the surface had LRO_x/LNO_x values greater than 0.35 (i.e., NO_x limited).

Figure 12 is similar to Figure 11 but with data from Houston. Here the typical photochemical environments in Galveston and Manvel Croix sites were both in the transition/ambiguous region during morning and midday but became NO_x limited by afternoon. Typical photochemical environments at the Deer Park, Channelview, West Houston, and Moody Tower sites (which typically experienced the highest surface O_3 mixing ratios) all remained in the transition/ambiguous region for the entire day (with inconsistent diurnal tendencies in $P(O_3)$ between these sites), while typical photochemical environments at Conroe and Smith Point were NO_x limited for the entire day with the highest $P(O_3)$ occurring in the morning. Previous surface-based studies conducted in summertime in Houston, such as the Texas Air Quality Study in 2000 (TexAQS, located 20 km southeast of the ship channel), the TexAQS II Radical and Aerosol Measurement Project in 2006 (TRAMP, located at Moody Tower), and the Study of Houston Atmospheric Radical Precursors in 2009 (SHARP, located at Moody Tower) indicated that $P(O_3)$ in Houston was generally radical limited in the morning hours and became more NO_x limited throughout the day [*Chen et al*., 2010; *Mao et al*., 2010; *Ren et al*., 2013]. *Ren et al*. [2013] noted that although $P(O_3)$ was radical limited in the morning during SHARP, the integrated O_3 production in the NO_x-limited regime (i.e., in the afternoon) was double that of the radical-limited regime, indicating that reductions in NO_x emissions would be most effective in reducing regional O_3 in Houston. Here we find that $P(O_3)$ at midday and afternoon at Moody Tower was typically much higher than in the morning (by nearly a factor of 3), and, although column CH_2O/NO_2 ratios have a large degree of uncertainty (i.e., a large transition/ambiguous range), similar information can still be derived by looking at the diurnal evolution of column CH_2O/NO_2 at Moody Tower. Even though our results indicate that column CH_2O/NO_2 ratios will not be able to differentiate between radical-limited and NO_x-limited regimes at Moody Tower at any time of day, the column CH_2O/NO_2 ratio tended to increase throughout the day. Therefore, one could still deduce that the abundance of radicals relative to NO_x also increases throughout the day, and the relative importance of NO_x as a limiting reagent in $P(O_3)$ also increases throughout the day—regardless of whether the region is actually NO_x limited or radical limited. Thus, even though we are unable to pigeonhole the time-dependent O_3 sensitivity at Moody Tower as being radical limited or NO_x limited, one could still deduce that reducing NO_x emissions, especially later in the day, would be effective for reducing local O_3. It should be noted, however, that our conclusions about $P(O_3)$ in Houston do not always agree with the results presented in a similar study, particularly in the morning [*Mazzuca et al*., 2016]. At Deer Park, for example, Mazzuca et al. reported a morning median $P(O_3)$ value of 30 ppbv/h, while we report a morning median value of 17.2 ppbv/h. This discrepancy is also present at every other site (with the exception of Galveston and Conroe), where our modeled $P(O_3)$ in the morning tends to be 5–10 ppbv/h lower than the reported values in *Mazzuca et al*. [2016]. This discrepancy can be attributed to differences in model chemistry: In a previous ground-based study conducted at Moody Tower, the Carbon Bond mechanism, version 5 (CB05, also used in *Mazzuca et al*. [2016]) was found to predict higher radical abundances than other mechanisms, including the LaRC box model [*Ren et al*., 2013]. This may be attributed to the simplified alkene chemistry used in CB05, which has been shown to lead to overpredictions of O_3 production in the morning in locations where alkenes dominate VOC reactivity (such as Deer Park) [*Heo et al*.,

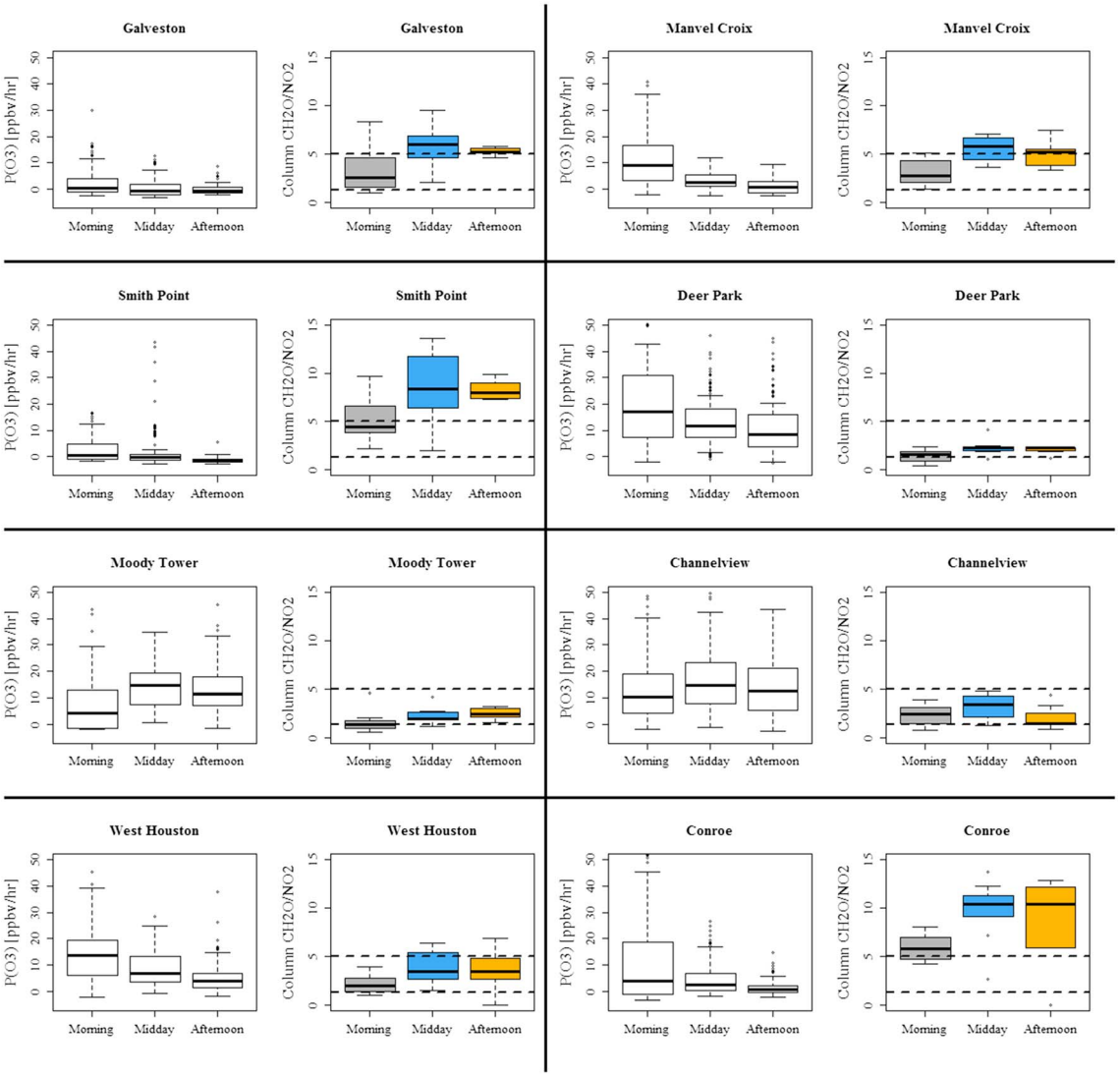

Figure 12. Box and whisker plots showing the median, 25th percentile, and 75th percentile of aircraft column CH_2O/NO_2 ratios and near-surface $P(O_3)$ (below 1 km) from each spiral site in Houston, binned by time of day. Here morning is defined as before 11:00 local time, midday as 11:00–13:30, and afternoon as after 13:30. The dashed horizontal lines represent the upper and lower limits of the column-based transition/ambiguous region (described in section 3.3 as spanning the range 1.3–5.0 in Houston).

2012]. Additional contributions to the discrepancy between our work and *Mazzuca et al*. [2016] include (1) Mazzuca et al. performed additional filtering of their data beyond what is stated in their text, which pushed their statistics toward more polluted air masses and (2) many of the VOCs used as model inputs in *Mazzuca et al*. [2016] were derived from Community Multiscale Air Quality Model (CMAQ) outputs (including some highly reactive species like ethene and propene), while our VOC inputs were entirely derived from airborne measurements (X. Ren, private communication, 2017).

In conclusion, observing the temporal behavior of column CH_2O/NO_2 may provide useful information about the photochemical environment (and which O_3 precursor species should be reduced to lower $P(O_3)$) even though we may not be able to index these measurements as radical limited or NO_x limited. This analysis demonstrates the potential utility of temporal monitoring that will be afforded by TEMPO, which is not possible using current satellite-based platforms such as OMI. Although the $P(O_3)$ reported here was calculated using our box model and aircraft data, recent work has suggested that column measurements of CH_2O may be proportional to near-surface $P(O_3)$ rates [*Schroeder et al*., 2016], indicating that all of the information contained in Figures 11 and 12 may be obtainable, to some degree, from geostationary satellites.

5. Summary and Conclusions

In this work, we have used a 0-D photochemical box model and data from DISCOVER-AQ to expand upon our current understanding of O_3 photochemistry, with an emphasis on broadening our understanding of the limitations associated with diagnosing near-surface O_3 sensitivity from satellite-based platforms. Our previous understanding of O_3 sensitivity was based on the assumption that the transition from a radical-limited to a NO_x-limited environment occurred at a LRO_x/LNO_x ratio of 1, but we found that the transition occurs at a ratio of 0.35. Although the primary loss mechanism for radicals changes at a ratio of 1 (from radical-radical interactions to radical-NO_x interactions), the instantaneous rate of O_3 production, which is more relevant for air quality purposes, reaches a maximum at a ratio of 0.35 due to the effect that additional NO_x imparts on OH concentrations. Under typical ambient conditions, the range of LRO_x/LNO_x spans multiple orders of magnitude, so the discrepancy that we note is unlikely to affect the primary findings of previous studies that used a ratio of 1, but future studies of O_3 sensitivity should take these results into consideration.

The fundamental work of *Martin* [2004] showed that satellite retrievals of CH_2O/NO_2 could be used to diagnose near-surface O_3 sensitivity, and an essential follow-up study by *Duncan et al*. [2010] expanded on this work and showed that there is a significant amount of uncertainty associated with this technique. Using existing data at the time, *Duncan et al*. [2010] were limited to quantifying the uncertainty of in situ CH_2O/NO_2 ratios to indicate in situ LRO_x/LNO_x ratios and could not explore additional uncertainty associated with using column CH_2O/NO_2 ratios to indicate near-surface LRO_x/LNO_x ratios. The DISCOVER-AQ data set is the first airborne data set to allow for statistically relevant calculation of the additional uncertainty associated with column CH_2O/NO_2 ratios as an indicator of near-surface O_3 sensitivity. In DISCOVER-AQ Colorado, we found a range of column CH_2O/NO_2 ratios between 1.1 and 3.0 that could not be reliably classified as either radical limited or NO_x limited, and instead are labeled as transition/ambiguous. This range of uncertainty is larger than that reported in *Duncan et al*. [2010], who found a transition/ambiguous range from 1.0 to 2.0. The increase in uncertainty is attributed to nonhomogeneous vertical distributions of CH_2O and NO_2 in the lower troposphere and the resulting fact that near-surface conditions may be decoupled from conditions at the top of the PBL and the lower free troposphere. In Houston, we found a transition/ambiguous range from 1.3 to 4.3, indicating that there is also regional variability in the ability of column CH_2O/NO_2 to indicate near-surface O_3 sensitivity. This regional variability suggests that follow-up studies must be performed to quantify the associated uncertainty in monitoring O_3 sensitivity from space in relevant regions, and that the results from one region are not likely to be applicable globally. Additionally, because each DISCOVER-AQ campaign was about 1 month long, we cannot comment on the role that seasonal variability may also play in affecting the associated uncertainty.

In addition to better quantifying the uncertainty associated with using satellite-based measurements to infer near-surface O_3 sensitivity, we also explored new air quality monitoring techniques that may be offered by future satellite-based platforms such as TEMPO. We showed that in Houston, the photochemical environment (as indicated by column CH_2O/NO_2) was significantly different on one extreme O_3 exceedance day (25 September 2013) than it was in the aggregate (month-long average). In the aggregate, most sites in Houston were NO_x limited, while CH_2O/NO_2 ratios were lower (mostly in the transition/ambiguous region) on 25 September. One distinct advantage of this type of monitoring is that the classifications of NO_x limited, radical limited, or transition/ambiguous become less important. For example, if one region has an aggregate CH_2O/NO_2 ratio of 4.5 that decreases to 2.0 on exceedance days, one can draw conclusions that the relative importance of (and abundance of) NO_x as an O_3 precursor increases on exceedance days, and that reducing NO_x emissions could be an effective pathway for reducing the number O_3 exceedance days. This difference in the indicated O_3 precursor environment during exceedance events could assist regulators who are looking to reduce the number of O_3 exceedance days. Additionally, we explored long-term averages of the column CH_2O/NO_2 ratio at morning, midday, and afternoon for sites in Colorado and Houston. The local O_3 sensitivity at some sites changed between NO_x limited, transition/ambiguous, and radical limited throughout the day, indicating that perhaps a time-dependent approach to reducing NO_x and/or VOC emissions could be employed to reduce integrated regional O_3 production.

While data collected during DISCOVER-AQ provide an ideal platform to better quantify the uncertainty associated with using column CH_2O/NO_2 to diagnose near-surface O_3 sensitivity, we must acknowledge that

additional uncertainty will result when translating these results to satellite measurements. For example, typical DISCOVER-AQ spirals extended to about 4 km above the surface, meaning that the free tropospheric contribution that we noted in this study is only a small representation of the entire free troposphere. While NO_2 tends to have negligible presence in the free troposphere, exceptions can occur in the outflow of convective storms and when regional/intercontinental transport is strong [*Brunner*, 1998; *Cooper et al*., 2009; *Crawford et al*., 2000]. In this work, we noted that there is a nonnegligible CH_2O presence in the free troposphere even under normal atmospheric conditions. Simply extrapolating our typical free tropospheric CH_2O mixing ratio up to 12 km (i.e., midlatitude tropopause height), we estimate an additional 0.1 Dobson units (DU) of CH_2O that is not accounted for in our DISCOVER-AQ spirals. However, as we showed in section 3, there can be small but significant variability in free tropospheric CH_2O, and it is likely that this estimate of 0.1 DU is not constant and varies from day to day. Another source of uncertainty is the satellite measurements themselves. Applying additional uncertainties of ±0.3 DU to CH_2O retrievals and ±0.03 DU to NO_2 retrievals, a pixel with CH_2O and NO_2 column densities of 1.0 DU would have a CH_2O/NO_2 ratio of 1.0 ± 0.34. Assuming a NO_2 column density of 1 DU and variable CH_2O, the associated transition/ambiguous range in Colorado would increase from 1.1–3.0 to 0.8–3.4 (a 37% increase in the transition/ambiguous range), while Houston would change from 1.4–4.3 to 1.1–4.7 (a 33% increase in the transition/ambiguous range). For regions with low CH_2O, this expansion of the transition/ambiguous range is likely to be even greater. Recent research has shown that the coarse-resolution models used to derive air mass factors for routine satellite trace gas retrievals often inadequately represent trace gas vertical distributions, leading to additional uncertainty and bias in routine satellite retrievals that was previously unaccounted for [*Liu et al*., 2016; *Valin et al*., 2011]. Additionally, while CH_2O is almost entirely contained within the troposphere, NO_2 has a nonnegligible presence in the stratosphere that has no impact on tropospheric chemistry. Accounting for variations in stratospheric NO_2 provides yet another source of uncertainty when using satellite retrievals of CH_2O/NO_2 to make inferences about lower tropospheric photochemical conditions. Evaluating tropospheric NO_2 retrievals against NO_2 column densities derived from DISCOVER-AQ aircraft spirals would provide an interesting follow-up study but is beyond the scope of this work.

Based on all of these additional sources of uncertainty (regional variability, seasonal variability, variable free tropospheric contributions, satellite retrieval uncertainty), we suggest that future studies that use satellite retrievals of CH_2O/NO_2 refrain from binning their data as radical limited, transition/ambiguous, or NO_x limited, as the range of uncertainty for a given location in space and time cannot be known without a detailed follow-up study. Instead, we suggest that future studies provide only the numerical value of column CH_2O/NO_2 ratios (or, perhaps more useful, long-term trends in column CH_2O/NO_2 ratios). Follow-up studies focused on exploring spatial and temporal variability in the relationship between CH_2O/NO_2 and near-surface O_3 sensitivity could include global modeling studies, aircraft studies, and surface-based studies that include colocated in situ and remote sensing instruments.

Acknowledgments
The authors would like to thank Glenn Diskin for providing measurements of CO and CH_4 and all members of the DISCOVER-AQ science team for executing this field project. All data used in this work can be downloaded from http://www-air.larc.nasa.gov/missions/discover-aq/discover-aq.html. PTR-MS measurements during DISCOVER-AQ were supported by the Austrian Ministry for Transport, Innovation, and Technology through the Austrian Space Applications Program (ASAP) of the Austrian Research Promotion Agency (FFG). Jason Schroeder and Tomas Mikoviny were partially supported by an appointment with the NASA Postdoctoral Program at NASA Langley Research Center, administered by Oak Ridge Associated Universities and Universities Space Research Association through contracts with NASA. Armin Wisthaler and Markus Müller received support from the Visiting Scientist Program of the National Institute of Aerospace (NIA). The authors would also like to thank Bryan Duncan, Brian Heikes, Luke Valin, and Heather Simon for useful comments that improved the quality of this paper.

References

Boersma, K. F., D. J. Jacob, M. Trainic, Y. Rudich, I. DeSmedt, R. Dirksen, and H. J. Eskes (2009), Validation of urban NO_2 concentrations and their diurnal and seasonal variations observed from the SCIAMACHY and OMI sensors using in situ surface measurements in Israeli cities, *Atmos. Chem. Phys.*, *9*(12), 3867–3879, doi:10.5194/acp-9-3867-2009.

Brunner, D. (1998), Large-scale nitrogen oxide plumes in the tropopause region and implications for ozone, *Science*, *282*(5392), 1305–1309, doi:10.1126/science.282.5392.1305.

Chameides, W., and J. C. C. G. Walker (1973), A photochemical theory of tropospheric ozone, *J. Geophys. Res.*, *78*(36), 8751–8760, doi:10.1029/JC078i036p08751.

Chameides, W. L., et al. (1992), Ozone precursor relationships in the ambient atmosphere, *J. Geophys. Res.*, *97*(D5), 6037–6055, doi:10.1029/91JD03014.

Chen, S., X. Ren, J. Mao, Z. Chen, W. H. Brune, B. Lefer, B. Rappenglück, J. Flynn, J. Olson, and J. H. Crawford (2010), A comparison of chemical mechanisms based on TRAMP-2006 field data, *Atmos. Environ.*, *44*(33), 4116–4125, doi:10.1016/j.atmosenv.2009.05.027.

Choi, Y., H. Kim, D. Tong, and P. Lee (2012), Summertime weekly cycles of observed and modeled NO_x and O_3 concentrations as a function of satellite-derived ozone production sensitivity and land use types over the continental United States, *Atmos. Chem. Phys.*, *12*(14), 6291–6307, doi:10.5194/acp-12-6291-2012.

Colorado Department of Public Health and Environment (CDPHE) (2008), Denver metro area & north front range 8-hour ozone State Implementation Plan (SIP) Technical Support Documents (TSD), appendix E, executive summary.

Colman, J., A. Swanson, S. Meinardi, D. R. Sive, B. Blake, and F. S. Rowland (2001), Description of the analysis of a wide range of volatile organic compounds in whole air samples collected during PEM-Tropics A and B, *Anal. Chem.*, *73*, 3723–3731.

Cooper, O. R., et al. (2009), Summertime buildup and decay of lightning NO_x and aged thunderstorm outflow above North America, *J. Geophys. Res.*, *114*, D01101, doi:10.1029/2008JD010293.

Crawford, J., et al. (1999), Assessment of upper tropospheric HO_x sources over the tropical Pacific based on NASA GTE/PEM data: Net effect on HO_x and other photochemical parameters, *J. Geophys. Res.*, *104*(D13), 16,225–16,273.
Crawford, J. H., et al. (2000), Evolution and chemical consequences of lightning-produced NO_x observed in the North Atlantic upper troposphere, *J. Geophys. Res.*, *105*(D15), 19,795–19,809, doi:10.1029/2000JD900183.
Duncan, B. N., et al. (2010), Application of OMI observations to a space-based indicator of NO_x and VOC controls on surface ozone formation, *Atmos. Environ.*, *44*(18), 2213–2223, doi:10.1016/j.atmosenv.2010.03.010.
Edwards, P. M., et al. (2013), Ozone photochemistry in an oil and natural gas extraction region during winter: Simulations of a snow-free season in the Uintah Basin, Utah, *Atmos. Chem. Phys.*, *13*(17), 8955–8971, doi:10.5194/acp-13-8955-2013.
Fishman, J., et al. (2008), Remote sensing of tropospheric pollution from space, *Bull. Am. Meteorol. Soc.*, *89*(6), 805–821, doi:10.1175/2008BAMS2526.1.
Flynn, C. M., et al. (2014), Relationship between column-density and surface mixing ratio: Statistical analysis of O_3 and NO_2 data from the July 2011 Maryland DISCOVER-AQ mission, *Atmos. Environ.*, *92*, 429–441, doi:10.1016/j.atmosenv.2014.04.041.
Fried, A., et al. (2011), Detailed comparisons of airborne formaldehyde measurements with box models during the 2006 INTEX-B and MILAGRO campaigns: Potential evidence for significant impacts of unmeasured and multi-generation volatile organic carbon compounds, *Atmos. Chem. Phys.*, *11*(22), 11,867–11,894, doi:10.5194/acp-11-11867-2011.
Fried, A., C. P. Loughner, and K. Pickering (2016), Analysis of airborne formaldehyde data over Houston Texas acquired during the 2013 DISCOVER-AQ and SEAC4RS campaigns.
Heo, G., E. McDonald-Buller, W. P. L. Carter, G. Yarwood, G. Z. Whitten, and D. T. Allen (2012), Modeling ozone formation from alkene reactions using the carbon bond chemical mechanism, *Atmos. Environ.*, *59*, 141–150, doi:10.1016/j.atmosenv.2012.05.042.
Jin, X., and T. Holloway (2015), Spatial and temporal variability of ozone sensitivity over China observed from the Ozone Monitoring Instrument, *J. Geophys. Res. Atmos.*, *120*, 7229–7246, doi:10.1002/2015JD023250.
Kleinman, L., Y. Lee, S. R. Springston, J. H. Lee, J. Weinstein-lloyd, and X. Zhou (1995), Peroxy radical concentration and ozone formation rate maximum radical production occurring near noon production of 8 ppb h^{-1} occurring EST. ozone accounts, *J. Geophys. Res.*, *100*(95), 7263–7273.
Kleinman, L. I. (1994), Low and high NO_x tropospheric photochemistry, *J. Geophys. Res.*, *99*(94), 831–838.
Kleinman, L. I. (2005), The dependence of tropospheric ozone production rate on ozone precursors, *Atmos. Environ.*, *39*(3), 575–586, doi:10.1016/j.atmosenv.2004.08.047.
Kleinman, L. I., P. H. Daum, J. H. Lee, Y. Lee, S. R. Nunnermacker, and L. Newman (1997), Dependence of ozone production on NO and hydrocarbons in the troposphere, *Geophys. Res. Lett.*, *24*(18), 2299–2302, doi:10.1029/97GL02279.
Liu, X., A. P. Mizzi, J. L. Anderson, I. Fung, and R. C. Cohen (2016), Assimilation of satellite NO_2 observations at high spatial resolution, *Atmos. Chem. Phys. Discuss.*, *2*, 1–18, doi:10.5194/acp-2016-770.
Mahajan, A. S., I. De Smedt, M. S. Biswas, S. Ghude, S. Fadnavis, C. Roy, and M. van Roozendael (2015), Inter-annual variations in satellite observations of nitrogen dioxide and formaldehyde over India, *Atmos. Environ.*, *116*, 194–201, doi:10.1016/j.atmosenv.2015.06.004.
Mao, J., et al. (2010), Atmospheric oxidation capacity in the summer of Houston 2006: Comparison with summer measurements in other metropolitan studies, *Atmos. Environ.*, *44*(33), 4107–4115, doi:10.1016/j.atmosenv.2009.01.013.
Martin, R. V. (2004), Space-based diagnosis of surface ozone sensitivity to anthropogenic emissions, *Geophys. Res. Lett.*, *31*, L06120, doi:10.1029/2004GL019416.
Martin, R. V., D. D. Parrish, T. B. Ryerson, J. K. Nicks, K. Chance, T. P. Kurosu, D. J. Jacob, E. D. Sturges, A. Fried, and B. P. Wert (2004), Evaluation of GOME satellite measurements of tropospheric NO_2 and HCHO using regional data from aircraft campaigns in the southeastern United States, *J. Geophys. Res.*, *109*, D24307, doi:10.1029/2004JD004869.
Mazzuca, G. M., X. Ren, C. P. Loughner, M. Estes, J. H. Crawford, K. E. Pickering, A. J. Weinheimer, and R. R. Dickerson (2016), Ozone production and its sensitivity to NO_x and VOCs: Results from the DISCOVER-AQ field experiment, Houston 2013, *Atmos. Chem. Phys.*, *16*(22), 14,463–14,474, doi:10.5194/acp-16-14463-2016.
McDuffie, E. E., et al. (2016), Influence of oil and gas emissions on summertime ozone in the Colorado northern front range, *J. Geophys. Res. Atmos.*, *121*, 8712–8729, doi:10.1002/2016JD025265.
Millet, D. B., D. J. Jacob, K. F. Boersma, T.-M. Fu, T. P. Kurosu, K. Chance, C. L. Heald, and A. Guenther (2008), Spatial distribution of isoprene emissions from North America derived from formaldehyde column measurements by the OMI satellite sensor, *J. Geophys. Res.*, *113*, D02307, doi:10.1029/2007JD008950.
Olson, J. R., et al. (2001), Seasonal differences in the photochemistry of the South Pacific: A comparison of observations and model results from PEM-Tropics A and B, *J. Geophys. Res.*, *106*(D23), 32,749–32,766, doi:10.1029/2001JD900077.
Olson, J. R., J. H. Crawford, G. Chen, W. H. Brune, I. C. Faloona, D. Tan, H. Harder, and M. Martinez (2006), A reevaluation of airborne HO_x observations from NASA field campaigns, *J. Geophys. Res.*, *111*, D10301, doi:10.1029/2005JD006617.
Parrish, D. D., et al. (2012), Primary and secondary sources of formaldehyde in urban atmospheres: Houston Texas region, *Atmos. Chem. Phys.*, *12*(7), 3273–3288, doi:10.5194/acp-12-3273-2012.
Ren, X., et al. (2013), Atmospheric oxidation chemistry and ozone production: Results from SHARP 2009 in Houston, Texas, *J. Geophys. Res. Atmos.*, *118*, 5770–5780, doi:10.1002/jgrd.50342.
Schroeder, J. R., L. L. Pan, T. Ryerson, G. Diskin, J. Hair, S. Meinardi, I. Simpson, B. Barletta, N. Blake, and D. R. Blake (2014), Evidence of mixing between polluted convective outflow and stratospheric air in the upper troposphere during DC3, *J. Geophys. Res. Atmos.*, *119*, 11,477–11,491, doi:10.1002/2014JD022109.
Schroeder, J. R., et al. (2016), Formaldehyde column density measurements as a suitable pathway to estimate near-surface ozone tendencies from space, *J. Geophys. Res. Atmos.*, *121*, 13,088–13,112, doi:10.1002/2016JD025419.
Sillman, S. (1995), The use of NO_y, H_2O_2, and HNO_3 as indicators for ozone-NO_x -hydrocarbon sensitivity in urban locations, *J. Geophys. Res.*, *100*(D7), 14,175–14,188, doi:10.1029/94JD02953.
Sillman, S., and D. He (2002), Some theoretical results concerning O_3-NO_x-VOC chemistry and NO_x-VOC indicators, *J. Geophys. Res.*, *107*(D22), 4659, doi:10.1029/2001JD001123.
Sillman, S., and P. J. Samson (1995), Impact of temperature on oxidant photochemistry in urban, polluted rural and remote environments, *J. Geophys. Res.*, *100*(D6), 11,497–11,508, doi:10.1029/94JD02146.
Sillman, S., J. Logan, and S. Wofsy (1990), The sensitivity of ozone to nitrogen oxides and hydrocarbons in regional ozone episodes, *J. Geophys. Res.*, *95*, 1837–1851, doi:10.1029/JD095iD02p01837.
Sillman, S., et al. (1995), Photochemistry of ozone formation in Atlanta, GA—Models and measurements, *Atmos. Environ.*, *29*(21), 3055–3066.
Sillman, S., D. He, M. R. Pippin, P. H. Daum, D. G. Imre, L. I. Kleinman, J. H. Lee, and J. Weinstein-Lloyd (1998), Model correlations for ozone, reactive nitrogen, and peroxides for Nashville in comparison with measurements: Implications for O_3-NO_x-hydrocarbon chemistry, *J. Geophys. Res.*, *103*, 22,629–22,644, doi:10.1029/98JD00349.

Simpson, I. J., et al. (2010), Characterization of trace gases measured over Alberta oil sands mining operations: 76 speciated C_2–C_{10} volatile organic compounds (VOCs), CO_2, CH_4, CO, NO, NO_2, NO_y, O_3, *Atmos. Chem. Phys.*, *10*(23), 11,931–11,954, doi:10.5194/acp-10-11931-2010.

Streets, D. G., et al. (2013), Emissions estimation from satellite retrievals: A review of current capability, *Atmos. Environ.*, *77*, 1011–1042, doi:10.1016/j.atmosenv.2013.05.051.

Thornton, J. A., et al. (2002), Ozone production rates as a function of NO_x abundances and HO_x production rates in the Nashville urban plume, *J. Geophys. Res.*, *107*(D12), 1–17, doi:10.1029/2001JD000932.

Tonnesen, G. S., and R. L. Dennis (2000), Analysis of radical propagation efficiency to assess ozone sensitivity to hydrocarbons and NO_x 2. Long-lived species as indicators of ozone concentration sensitivity, *J. Geophys. Res.*, *105*(D7), 9227–9241, doi:10.1029/1999JD900372.

U.S. Environmental Protection Agency (US EPA) (2008), Implementation of the 2008 National Ambient Air Quality Standards (NAAQS) for ozone: State Implementation Plan (SIP) requirements. [Available at https://www.epa.gov/ozone-pollution/implementation-2008-national-ambient-air-quality-standards-naaqs-ozone-state.]

U.S. Environmental Protection Agency (US EPA) (2015), National ambient air quality standards for ozone.

U.S. Environmental Protection Agency (US EPA) (2016), Implementation of the 2015 National Ambient Air Quality Standards for Ozone: Nonattainment Area Classifications and State Implementation Plan Requirements, Environmental Protection Agency, Washington, D. C.

Valin, L. C., A. R. Russell, R. C. Hudman, and R. C. Cohen (2011), Effects of model resolution on the interpretation of satellite NO_2 observations, *Atmos. Chem. Phys.*, *11*(22), 11,647–11,655, doi:10.5194/acp-11-11647-2011.

Valin, L. C., M. Fiore, A. K. Chance, and G. González Abad (2015), The role of OH production in interpreting the variability of CH_2O columns in the southeast U.S, *J. Geophys. Res. Atmos.*, *121*, 3510–3532, doi:10.1002/2015JD024012.

Witte, J. C., B. N. Duncan, A. R. Douglass, T. P. Kurosu, K. Chance, and C. Retscher (2011), The unique OMI $HCHO/NO_2$ feature during the 2008 Beijing Olympics: Implications for ozone production sensitivity, *Atmos. Environ.*, *45*(18), 3103–3111, doi:10.1016/j.atmosenv.2011.03.015.

Wolfe, G. M., et al. (2015), Formaldehyde production from isoprene oxidation across NO_x regimes, *Atmos. Chem. Phys. Discuss.*, *15*(21), 31,587–31,620, doi:10.5194/acpd-15-31587-2015.

Wolfe, G. M., et al. (2016), Formaldehyde production from isoprene oxidation across NO_x regimes, *Atmos. Chem. Phys.*, *16*(4), 2597–2610, doi:10.5194/acp-16-2597-2016.

Xie, M., K. Zhu, T. Wang, H. Yang, B. Zhuang, S. Li, M. Li, X. Zhu, and Y. Ouyang (2014), Application of photochemical indicators to evaluate ozone nonlinear chemistry and pollution control countermeasure in China, *Atmos. Environ.*, *99*, 466–473, doi:10.1016/j.atmosenv.2014.10.013.